



## Triple-functional bone adhesive with enhanced internal fixation, bacteriostasis and osteoinductive properties for open fracture repair

Yusheng Yang<sup>a,1</sup>, Shenghui Su<sup>b,1</sup>, Shencai Liu<sup>c,1</sup>, Weilu Liu<sup>c</sup>, Qinfeng Yang<sup>c</sup>, Liangjie Tian<sup>a</sup>, Zilin Tan<sup>d</sup>, Lei Fan<sup>c</sup>, Bin Yu<sup>a,\*\*\*</sup>, Jian Wang<sup>c,\*\*</sup>, Yanjun Hu<sup>a,\*</sup>

<sup>a</sup> Division of Orthopaedics and Traumatology, Department of Orthopaedics, Nanfang Hospital, Southern Medical University, Guangzhou, Guangdong Province, 510515, China

<sup>b</sup> Department of Orthopaedics, Ningde Municipal Hospital, Ningde Normal University, Ningde, Fujian Province, 352100, China

<sup>c</sup> Division of Orthopaedics Surgery, Department of Orthopaedics, Nanfang Hospital, Southern Medical University, Guangzhou, Guangdong Province, 510515, China

<sup>d</sup> Department of General Surgery, Nanfang Hospital, Southern Medical University, Guangzhou, Guangdong Province, 510515, China

### ARTICLE INFO

#### Keywords:

Open fracture  
Bone adhesive  
Internal fixation  
Bacteriostasis  
Osteoinduction

### ABSTRACT

At present, effective fixation and anti-infection implant materials represent the mainstay for the treatment of open fractures. However, external fixation can cause nail tract infections and is ineffective for fixing small fracture fragments. Moreover, closed reduction and internal fixation during the early stage of injury can lead to potential bone infection, conducive to bone nonunion and delayed healing. Herein, we designed a bone adhesive with anti-infection, osteogenic and bone adhesion fixation properties to promote reduction and fixation of open fractures and subsequent soft tissue repair. It was prepared by the reaction of gelatin (Gel) and oxidized starch (OS) with vancomycin (VAN)-loaded mesoporous bioactive glass nanoparticles (MBGNs) covalently cross-linked with Schiff bases. Characterization and adhesion experiments were conducted to validate the successful preparation of the Gel-OS/VAN@MBGNs (GOVM-gel) adhesive. Meanwhile, *in vitro* cell experiments demonstrated its good antibacterial effects with the ability to stimulate bone marrow mesenchymal stem cell (BMSCs) proliferation, upregulate the expression of alkaline phosphatase (ALP) and osteogenic proteins (RunX2 and OPN) and enhance the deposition of calcium nodules. Additionally, we established a rat skull fracture model and a subcutaneous infection model. The histological analysis showed that bone adhesive enhanced osteogenesis, and *in vivo* experiments demonstrated that the number of inflammatory cells and bacteria was significantly reduced. Overall, the adhesive could promote early reduction of fractures and antibacterial and osteogenic effects, providing the foothold for treatment of this patient population.

### 1. Introduction

Open fractures have a high incidence of postoperative complications [1,2]; the main clinical treatment method is debridement in the early post-traumatic period to control the contaminated or infected wound in a near-sterile environment and for effective fixation and closure of open fractures [3–5]. However, infection rates of up to 27% have been reported following the reduction of severe open fractures involving the lower limb [6], even with thorough debridement during the golden

period of 6–8 h after fractures [7]. When infected with bacteria, the fractured regions, including those underlying soft tissues, cease to heal, resulting in a reduction in blood supply and an inability to regenerate bone [8]. The self-healing capacity and bone regeneration may be inhibited due to the lack of blood supply and systemic antibiotics [9]. Importantly, many bone implantable biomaterials with antibiotics (i.e., clindamycin gentamicin, vancomycin) and bone cement, including calcium phosphate, calcium sulfate, and PMMA, can reportedly prevent bacterial infection at local defect sites while promoting bone repair [8,

Peer review under responsibility of KeAi Communications Co., Ltd.

\* Corresponding author.

\*\* Corresponding author.

\*\*\* Corresponding author.

E-mail addresses: [yubinol@163.com](mailto:yubinol@163.com) (B. Yu), [nfywj@126.com](mailto:nfywj@126.com) (J. Wang), [huyanjun4750@smu.edu.cn](mailto:huyanjun4750@smu.edu.cn) (Y. Hu).

<sup>1</sup> The first three authors contributed equally to this work.

<https://doi.org/10.1016/j.bioactmat.2023.01.021>

Received 2 November 2022; Received in revised form 18 January 2023; Accepted 28 January 2023

2452-199X/© 2023 The Authors. Publishing services by Elsevier B.V. on behalf of KeAi Communications Co. Ltd. This is an open access article under the CC BY-NC-ND license (<http://creativecommons.org/licenses/by-nc-nd/4.0/>).

10–12]. It is widely thought that calcium cement, such as calcium sulfate, superphosphate, and calcium triglyceride, can stimulate bone regeneration [13]. However, these bone implantable biomaterials exhibit limited ability to effectively fix the fracture fragments, increasing the incidence of delayed union, nonunion and malunion [14, 15]. Overall, fixation is also a key factor for the crucial application of implants in the open fracture.

Stabilizing open fracture fragments is critical to successfully healing open fractures [14,16]. Currently, external fixators represent the most commonly used fixation method in open fractures, indicated for treating periarticular unstable fractures, fractures with severe soft tissue damage [17], floating knee injuries [18], or, most commonly, in treating compound fractures at the diaphysis level. External fixators bring the advantages of exerting a minimal effect on the blood supply of fracture fragments and little soft tissue injury, and the wound is limited to the nail tract, which reduces the risks of infection [19]. Moreover, the external fixator can reduce stress shielding of stirless locking fixation and regulate the longitudinal axis of the shaft [20–23]. Compression, stretch, and neutral fixation are performed based on the open fracture type. But more importantly, segmental fractures and comminuted fractures with very small fracture fragments cannot be effectively fixed. At the same time, the healing process is long, and the procedure is often costly and time-consuming. Although internal fixation can solve the above problems, it can also cause catastrophic infection of deep tissue and serious complications such as chronic osteomyelitis, tissue necrosis, amputation, etc. [24,25]. Hence, designing a kind of bone adhesive for early reduction and internal fixation to flexibly cohere and effectively fix fracture fragments and subsequently promote bone regeneration and antibacterial during fracture healing is urgently needed for medical progress.

In this study, we designed an injectable antibacterial and osteogenic bone adhesive for application during the fixation of open fracture fragments (Fig. 1). The adhesive met various material performance

requirements. It promoted the reduction and internal fixation of open fractures and exhibited good degradability in vivo [26], reducing the hassle of removing metal implants later. Besides, it demonstrated good moldability and could be shaped to meet the needs of different fractures with bacteriostatic and osteogenic effects. Last but not least, it was relatively easy to use and decreased the duration of surgery. In the present study, oxidized starch (OS) and modified methacrylate gelatin (Gel) were first cross-linked to obtain a biodegradable and adhesive hydrogel that could adhere to tissues for stable fixation of fracture fragments. At the same time, vancomycin (VAN) was delivered via a distinct nano-carrier made of mesoporous bioactive glass nanoparticles (MBGNs). MBGNs have been shown to promote osteogenesis and angiogenesis [27–32]. In addition, MBGNs can modulate hydrogel degradation and enhance its mechanical properties by control of cross-linking, surface modification, and bioactive filler incorporation [14]. Finally, we mixed them to obtain the adhesive Gel-OS/VAN@MBGNs (GOVM-gel).

Herein, we first examined the adhesion ability of GOVM-gel. Then, we assessed the adhesion effect of the bone adhesive to the fracture by mechanical tests. Drug susceptibility tests were conducted to analyze the anti-bacterial activity against staphylococcus aureus and demonstrate its efficacy in a rat subcutaneous bacteria-infection model. Last, in vitro osteogenesis experiments and rat calvarial open fracture models were conducted to evaluate the material's bone repair and regeneration ability. Overall, GOVM-gel provides a new option to promote reduction and internal fixation, exhibiting antibacterial and osteogenic properties in open fractures and can hopefully be applied in other medical areas.

## 2. Materials and methods

### 2.1. Materials and reagents

The materials and reagents were obtained from Aladdin (Shanghai,

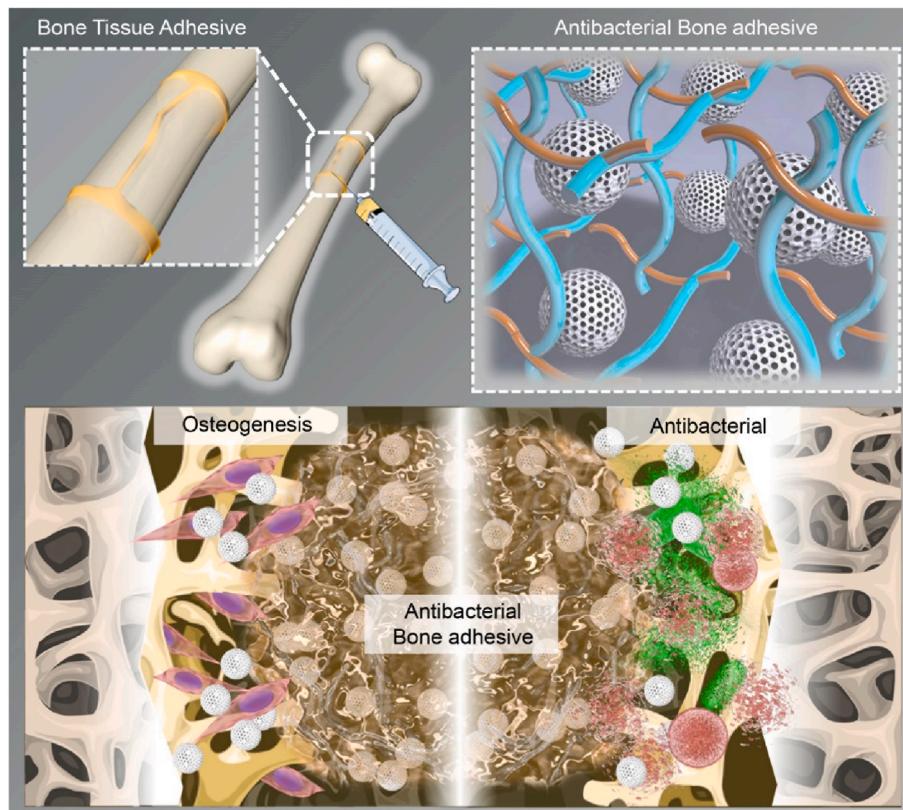


**Fig. 1.** Schematic diagram of treatment principle. The Gel-OS/VAN@MBGNs (GOVM-gel) can fix fragments during surgical open fracture treatment by releasing VAN and promotes bone regeneration.

China), including Gel (M299511-5g), sodium periodate (AR,  $\geq 99.5\%$ ), Tetraethyl orthosilicate (TEOS, AR, 98%), Methylene blue and ammonia solution (AR, 25–28%). We bought hexadecyl trimethyl ammonium bromide (CTAB, AR,  $\geq 99\%$ ) from Fangyuan Biotechnology Co., Ltd., and Ethyl acetate (EA, AR,  $\geq 99.5\%$ ) was purchased from the Guangdong Huaying Technology Co. Ltd. Calcium nitrate (CN, AR, 99%) was from Tianjin Fuchen Chemical Reagent Factory. VAN was purchased from Shanghai Technology Co. Ltd (Shanghai, China). CCK-8 kits were bought from Beyotime Biotechnology Co., Ltd (Shanghai, China). The OPN and RunX2 antibodies were purchased from Abcam (Shanghai, China). In addition, we purchased cell staining reagents, including  $\beta$ -Actin, Calcein-AM, PI, Hoechst, SYTO 9, FITC, and phosphate-buffered saline (PBS). Meanwhile, DMEM, RPMI-1640, and fetal bovine serum (FBS) for cell experiments were bought from Gibco.

## 2.2. Cells and animals

RAW264.7 cells were provided by Southern Medical University (Guangzhou, China). Bone marrow mesenchymal stem cell (BMSCs) were extracted from rat bone marrow tissue. SD rats (male, 250–300 g) were purchased from Southern Medical University's animal experiment management center. All animal experiments were carried out in the Animal Experimental Center of Nanfang Hospital. All operations were trained, and the experimental protocol was reviewed and approved by the Ethics Committee of Southern Medical University.

## 2.3. Sample preparation

### 2.3.1. Preparation of OS

The OS was prepared as described in the literature [33–35]. First, 10.56% sodium (w/v) periodate was combined with aqueous starch solution in a 1:1 ratio, and the mixture was kept in the dark for 2.5 h at room temperature. Then the oxidized products were precipitated using a certain percentage of ethanol. The oxidation of starch was evaluated using Fourier transform infrared spectroscopy (FTIR) spectroscopy.

### 2.3.2. Synthesis of MBGNs

The synthesis of MBGNs was conducted as previously documented [36–38]. First, 5.0 g of CTAB was completely dissolved in 240 mL water at room temperature while stirring. The CTAB solution was then mixed with ethyl acetate for 40 min. Next, we added 50 mL of a 1 mol/L ammonia solution to the aqueous solution and stirred it for 15 min. After adding TEOS and CN, the mixture was stirred for an additional 40 min. We obtained MBGNs through several steps, including centrifugation, water washing, alcoholization, drying, and grinding. The surface morphology of mesoporous bioactive glass nanoparticles was examined using a scanning electron microscope (SEM) and transmission electron microscope (TEM). A Malvern Nano-ZS 90 laser particle size analyzer was used to examine the size distribution of MBGNs. The chemical structure and phase of MBGNs were analyzed using FTIR.

### 2.3.3. Synthesis and characterization of GOVM-gel

First, VAN and MBGNs were mixed to prepare VAN-loading MBGNs (5% w/v). The OS was added into an aqueous solution to form an OS mixture solution (10% w/v) and mixed with the MBGNs solution, which was prepared earlier. After ultrasonication for 15 min at room temperature, MBGNs were mixed with the OS solution. Subsequently, we mixed OS/VAN@MBGNs (OVM) with Gel to form the GOVM-gel molded in a round shape. Finally, we analyze the chemical structure of the GOVM-gel by FTIR. Meanwhile, the adhesive was poured into a stainless-steel mold and then frozen at  $-20\text{ }^{\circ}\text{C}$  for 1 h,  $-80\text{ }^{\circ}\text{C}$  for 2 h, and finally lyophilized in a freeze-dryer (Labconco., USA) for 48 h to obtain the dehydrated sample. The surface morphology of the GOVM-gel was examined under a SEM.

### 2.3.4. VAN release capacity of GOVM-gel

VAN with a concentration of 0.15 mg/ml was encapsulated in the hydrogel, and then 5 mL PBS buffer was added to it. The solution was incubated at  $37\text{ }^{\circ}\text{C}$  and shaken at 100 rpm. The supernatant was collected at intervals to test the solution drug concentration. In addition, the release performance of the drug in hydrogels was evaluated by calculating the cumulative release percentage of the drug in each time period.

## 2.4. Biological and mechanical properties of GOVM-gel

### 2.4.1. Rheological studies

The rheology of hydrogel was studied and analyzed by a DHR-2 rotary rheometer. In all studies, 40 mm circular parallel plates were used, the temperature was set at  $25\text{ }^{\circ}\text{C}$ , the angular velocity was set at 10 rad/s and the amplitude scan started from a 10-1 strain rate to measure loss modulus ( $G''$ ) and storage modulus ( $G'$ ) of different hydrogels.

### 2.4.2. The setting time of GOVM-gel

Using the vial inversion method, the setting time of adhesives with different formulations was evaluated. Briefly, 2 mL of Gel and 2 mL OS/VAN@MBGNs mixture were added to two transparent glass bottles. The glue was allowed to cure at room temperature. The setting time was defined when the gel solution stopped flowing when the vials were tilted.

### 2.4.3. Injectability studies

OVM and the Gel solution were put in two syringes, respectively, and OVM were labelled with methylene blue. Then, OVM were mixed with the gel solution through a three-way tube and injected into an aqueous solution to observe its injectability.

### 2.4.4. Self-healing performance

To assess the bone adhesive's self-healing capability, the test was carried out by cutting two adhesives that had completely hardened into tablet form and been dyed with two different colors into halves; the blue bone adhesive was mixed with methylene blue and then reconnected them after exchanging one bone fragment between the two pairs. After allowing the samples to heal for 20 min, they were subjected to tensile stress with tweezers to rejoin samples.

### 2.4.5. Adhesive strength of adhesives and tensile mechanical test

To assess whether adhesives could stick to bone fragment tissue, fresh pieces of porcine cancellous bone were cut from pork femurs and ribs bought from a local butcher. First, we injected 100 mL of adhesive into the two bone slices and rejoined them in end-to-end and lap-shear manners. Next, we applied the adhesive to the femoral head's two bone fragments left at room temperature for 30 min to fully solidify. Last, we conducted a tensile mechanical test to find the maximum stress of the bonded joint before it breaks in end-to-end direction and lap-shear surface. In addition, a pig femoral head was sawed off for further characterization of the adhesiveness strength; the broken ends were then glued together. After 30 min, a bucket containing 3 L of water was hung under the femoral head to test the maximal adhesive strength before the failure of the adhesive. Next, we separated them and reconnected them to test the tension. Moreover, we rotated them  $180^{\circ}$  to further test the tensile strength.

## 2.5. Biocompatibility testing

### 2.5.1. Cell live/dead staining

BMSCs were cultured for the experimental assay. The cells were inoculated into 3-cm culture dishes and co-cultured with the hydrogel prepared from the material for 24 h. After that, the cells were washed thrice with PBS, digested with trypsin for 3 min, suspended by adding complete medium and then transferred to a centrifuge tube for

precipitation (1000 rpm, 5 min). After discarding the supernatant, PBS was used to wash the cells three times, and a cell suspension was obtained. 100  $\mu$ L of staining solution was added to 200  $\mu$ L of the cell suspension, which was subsequently incubated at room temperature for 20 min. A fluorescent microscope was used to observe cell death using 490 nm excitation light.

### 2.5.2. Cell proliferation assay

BMSCs from 4-week-old male SD rats were incubated at 37 °C in a 5% carbon dioxide incubator. The basic composition of the DMEM medium included 6% FBS and 1% penicillin-streptomycin double antibiotics. The 96-well plate was inoculated with 100  $\mu$ L of  $5 \times 10^3$  density cell suspension per well and then incubated in the incubator for 24 h. 10  $\mu$ L of material samples were added to each of the blank and experimental groups, and incubation was continued for 12 h. 10  $\mu$ g CCK-8 reagent was added to each well and incubated for 4 h. The absorbance at 450 nm was measured with an enzyme marker to assess the cell status.

### 2.5.3. Cell spreading area

BMSCs were first extracted from the bone marrow cavity of SD rats and then seeded onto the bone adhesive at a density of  $1 \times 10^4$  per well and cultured for different time durations. After  $\beta$ -Actin and Hoechst staining, confocal laser scanning microscopy (CLSM) was used to observe the cytoskeleton. We used ImageJ 1.8.0 to quantify cell spreading based on CLSM imaging of the three groups.

### 2.5.4. In vivo compatibility of GOVM-gel

After placing the adhesive on the fractured end of the rat for a specific duration, the major organs, including the heart, liver, spleen, lung and kidney of the animal, were harvested and underwent histological analysis and blood was drawn to detect the liver function, kidney function and blood routine, and to observe the biological toxicity of the adhesive by the Hemolysis test.

### 2.6. Degradation tests of GOVM-gel

To further evaluate the degradation rate of GOVM-gel in vivo and in vitro, the adhesive was immersed in 5 mL PH 7.4 PBS and was continuously shaken in a shaker at room temperature. The hydrogel was washed and weighed every 3 days. At the same time, to evaluate the degradation behavior of hydrogel in vivo, the hydrogel was mixed with Cy 7.0 fluorescence, and the two were combined by a covalent hydrogen bond. The GOVM-gel (2 mL) and Cy7.0 fluorescence mixture was injected subcutaneously into rats, and the fluorescence signal was observed and recorded every 7 days by an in vivo imager. In addition, the fluorescent hydrogel was injected into the skull fracture site of rats to observe its degradation at the fracture site and comprehensively evaluate its biodegradation behavior.

### 2.7. In vitro antibacterial properties of the hydrogel

#### 2.7.1. Antibacterial rate

$1 \times 10^8$  cfu/mL *Staphylococcus aureus* solution was obtained, diluted over a gradient to  $1 \times 10^5$  cfu/mL, and inoculated into 10 cm Petri dishes containing culture solutions from the experimental and the control groups for a total of 24 h. The culture solution was then inoculated onto sterile agar plates with diluted inoculation rings. After incubation in a bacterial incubator at 37 °C for 24 h, the number of colonies was counted.

#### 2.7.2. Inhibition zone

The  $1 \times 10^4$  bacterial solution was coated into MH agar plates, and two groups of sterile drug-sensitive tablets were soaked in saline and VAN for 15 min and then placed on the agar plates, and the remaining two groups were each placed on Gel-OS@MBGNs (GOM) and GOVM-gel. The agar plates were incubated at 37 °C for 24 h to observe the

inhibition zone size and the antimicrobial effect of the material.

#### 2.7.3. Bacterial live/dead staining

*Staphylococcus aureus* was cultured in nutrient broth and allowed to grow to the log phase. Centrifugation at 10,000g was performed for 15 min, and the bacterial culture was concentrated. The supernatant was aspirated, and 3 mL of PBS was added to it to resuspend the bacterial suspension. 1 mL of the bacterial suspension was added to PBS, VAN, GOM and GOVM-gel, respectively. After 1 h, centrifugation was conducted to precipitate the resuspension. Equal amounts of mixed staining solution components A and B were added to every 1 mL bacterial suspension and incubated at room temperature under dark conditions. Finally, the bacterial solution was dropped onto a slide to observe the fluorescence intensity.

### 2.8. In vitro osteogenesis assay of the hydrogel

#### 2.8.1. ALP staining

ALP kits were used to detect the osteogenic index of BMSCs cultured in different hydrogels. The fluorescence values were then measured under a fluorescent enzyme marker to determine the osteogenic index.

#### 2.8.2. Alizarin Red S (ARS) staining

The cells were placed in an osteogenic medium for 14 days, after which the culture medium was discarded and washed with PBS. Next, 4% paraformaldehyde was used for cell fixation for 15 min. The fixative was washed with PBS, and ARS staining was added for 30 min. Finally, the calcium salt content was quantified by recording the optical density value at 570 nm under the enzymatic standard.

#### 2.8.3. Real-time (RT)-PCR experiments

Total RNA was extracted from the cells using the Trizol reagent after culturing for 14 days. Then a reverse transcription kit was used to reverse-transcribe RNA into cDNA (Table S1). The Maxima™ SYBR Green/ROX qPCR Master Mix was used to perform RT-PCR. All experiments were performed in triplicates.

#### 2.8.4. Western blot

A protein extraction kit was used to extract the proteins, and cells were lysed in protease inhibitors and phosphatase inhibitors. The BCA protein Kit was used to determine the protein concentrations. The proteins were loaded onto SDS gels, separated by electrophoresis for 80 min, and then transferred onto PVDF membranes for 2 h. Finally, they were blocked with milk and incubated with primary antibodies overnight. After washing with TBST thrice, incubation with the secondary antibodies was conducted for 60 min at room temperature, and the protein was added to an ECL chromogenic solution [39]. The results were analyzed with Image J software, and the gray values of serum protein bands were calculated.

#### 2.8.5. Immunostaining

Following the culture of BMSCs for 14 days, PBS was used to wash the cells thrice, followed by fixation with 4% paraformaldehyde at room temperature for 30 min. Subsequently, we incubated the cells in 0.1% TritonX-100 in PBS for 15 min at room temperature. Blocking was conducted with 1% BSA in PBS during 2 h. After incubation with primary antibodies (anti-OPN and anti-RunX2) (Table S2) at 4 °C overnight, the cells were washed thrice with PBS and incubated with secondary goat anti-mouse IgG, which is conjugated with Alexa-Fluor 594. After washing, Hoechst was used to stain the cell nuclei for 15 min. A confocal microscope was used to capture the images [40].

## 2.9. Animal experiments

### 2.9.1. Subcutaneous infection model in rats

Eight-week-old rats were anesthetized, and their backs were shaved and disinfected. Incisions of approximately 7 mm were made symmetrically along the middle of the spine on both sides. We made round adhesives with a diameter of 5 mm by placing 300  $\mu\text{L}$  samples in a circular mold; these adhesives were then placed under the skin of animals. 200  $\mu\text{L}$  of  $1 \times 10^8$  cfu/mL *Staphylococcus aureus* suspension was injected with a 1 mL syringe. The incisions were sutured and disinfected with alcohol, and the animals were executed one week later for histological analysis.

### 2.9.2. Rat open cranial fracture model

7–8 weeks old SD male rats were selected and anesthetized with sodium isobarbital intraperitoneally (1 mL/100 g of 0.3% sodium pentobarbital). A 4-mm diameter hole was drilled into the top of the rat's skull using a microporous drill, into which vancomycin-laden bioactive glass hydrogel was injected. Four weeks later, the animals were executed and removed for imaging Micro-CT examination and histological HE and Masson section staining. All experiments were approved by Nanfang Hospital of Southern Medical University.

## 2.10. Statistical analysis

All quantitative data were expressed as the mean  $\pm$  standard deviation (SD). All experiments in this study were performed at least three times. Differences between the experimental and control groups were determined using a one-way analysis of variance. Differences were considered significant at (\*)  $p < 0.05$ , (\*\*)  $p < 0.01$  and (\*\*\*)  $p < 0.001$ . GraphPad Prism 8 and Origin Pro 2021 were used for statistical analysis and data processing.

## 3. Results and discussion

### 3.1. Screening for sensitive antibiotics from clinical patient specimens

The most common pathogen associated with open fracture infection is reportedly *Staphylococcus aureus* [41]. In the present study, five cases of refractory and recurrent bone infections caused by *Staphylococcus aureus* were collected and tested for drug susceptibility. A white precipitate  $>0.2$  mm indicated that the antibiotic was not sensitive to pathogenic bacteria (Fig. 2a). We found that *Staphylococcus aureus* in 5 samples was sensitive to antibiotics, including VAN and teicoplanin (TEC) (Fig. 2a). In addition, a precipitate was observed at a concentration of 8  $\mu\text{g}/\text{mL}$  TEC, but not with VAN, which substantiated that VAN had a lower minimum inhibitory concentration (MIC) than TEC. Consistently, heat map quantitative analysis showed that VAN was the most suitable antibiotic (Fig. 2b). An increasing body of evidence suggests that VAN is sensitive to *Staphylococcus aureus* at a MIC of 4  $\mu\text{g}/\text{mL}$  and moderately sensitive when the MIC exceeds 4  $\mu\text{g}/\text{mL}$  and is lower than 16  $\mu\text{g}/\text{mL}$  [42–44]. We found that 8  $\mu\text{g}/\text{mL}$  VAN exhibited a good safety profile with minimal nephrotoxicity and hepatotoxicity, which provides a good basis for clinical guidance in treating refractory bone infections. To validate the MIC of VAN, agar plate experiments were carried out, and a large number of bacteria were observed on the agar plate at concentrations of 2  $\mu\text{g}/\text{mL}$  and 4  $\mu\text{g}/\text{mL}$ , while the bacteria were killed at concentrations of 8  $\mu\text{g}/\text{mL}$  and 16  $\mu\text{g}/\text{mL}$  (Fig. 2c–d). In addition, the results of the antibacterial activity by inhibition zone estimation showed that 8  $\mu\text{g}/\text{mL}$  and 16  $\mu\text{g}/\text{mL}$  yielded a good antibacterial effect (Fig. 2e), with comparable inhibition zones (Fig. 2f), which may be related to the time-dependent effect of VAN rather than being concentration-dependent [45]. Many bacteria died at 8  $\mu\text{g}/\text{mL}$  during bacterial live/dead staining (Fig. 2g). In summary, we observed the optimal bactericidal effect of vancomycin at 8  $\mu\text{g}/\text{mL}$ . Indeed, VAN has been established as an important antibiotic against drug-resistant

*Staphylococcus aureus* and other pathogens [45]. An effective drug concentration is required to yield optimal bactericidal effects.

### 3.2. Fabrication and characterization of GOVM-gel

Gelatin is a water-soluble biopolymer. Unlike GelMa, gelatin is capable of dynamically and reversibly binding with OS because of its unique active amino acid sequence, making it a widely used material in tissue engineering [63]. Gelatin, OS and MBGNs were manufactured as previously documented, to create GOVM-gel [32,33,37], as shown in Fig. 3a. Fourier transform infrared (FTIR) analysis demonstrated a newly wave infrared band at  $1750\text{ cm}^{-1}$  in the spectrum of starch (Fig. S3), which corresponded to the stretching vibration of aldehyde groups, confirming the oxidization of starch. Growing evidence suggests that MBGNs have a granular structure similar to mesoporous silicate [36,46] and its chemical composition is  $85\text{SiO}_2\text{-}15\text{CaO}$  (mol%) [36]. MBGNs can effectively enhance the interaction between the structure of chemical substances [47,48], increasing the strength of the bond formation. In our study, SEM was used to observe the structure of MBGNs (Fig. 3b–c). TEM revealed that these microspheres had a porous structure (Fig. 3d). Malvern Nano zetasizer further validated that the diameter of MBGNs ranged from 100 to 200 nm (Fig. 3e). Next, 8  $\mu\text{g}/\text{mL}$  VAN was incorporated into MBGNs to prepare VAN@MBGNs. At  $37\text{ }^\circ\text{C}$ , Gel (30% (w/v)) and OS (10% (w/v)) containing VAN@MBGNs (5% (w/v)) were combined to produce GOVM-gel, and a new absorption peak was observed in the FTIR spectra of starch at  $1660\text{ cm}^{-1}$  (Fig. 3f), confirming the formation of gel [49]. Moreover, we observed an absorption peak at  $810\text{ cm}^{-1}$  and a broad peak at  $1000\text{--}1300\text{ cm}^{-1}$  in the FTIR spectra of mesoporous bioactive glass nanoparticles, reflecting the asymmetric vibrations of Si-O-Si and Si-O- bonds. In addition, the vial inversion test substantiated that the material exhibited good gel-forming properties (Fig. 3g). The hydrogel gelling process was studied using a dynamic time sweep rheological experiment. The crossovers of loss modulus ( $G''$ ) and storage modulus ( $G'$ ) indicated gelling of the GOVM-gel (Fig. 3h). At the same time, we measured the modulus of hydrogels after adding different contents of MBGNs to characterize their surface stiffness (Fig. S4). The mechanical properties of GOVM-gel were significantly improved when MBGNs were added, demonstrating their role as cross-linking agents. It has been reported that three mechanisms may lead to GOVM-gel formation [49]. First, it is highly conceivable that Schiff bases, primarily responsible for the synthesis of hydrogels, are formed by the free amino groups forming the gel and the aldehyde groups in oxidized starch [50]. The formation of Schiff bases between Gel and OS is indicated by the elimination of the band at  $1730\text{ cm}^{-1}$  and the emergence of a strong peak of 1725 and  $1600\text{ cm}^{-1}$  in the FTIR spectra of GOVM-gel. Moreover, the development of Schiff's base may be accelerated by an alkaline pH [51]. Furthermore, MBGNs can also quickly establish an alkaline environment in the medium, thereby enhancing the production of Schiff's bases and speeding the formation of hydrogels. Moreover, during the hydration process, a cluster of silanol groups (Si-OH) may develop on the surface of MBGNs in an aqueous environment, and they can interact with amino groups and carboxyl groups on Gel-OS to form hydrogen bonds, therefore strengthening the cross-linking [37]. Importantly, the GOVM-gel precursor could be easily injected using a syringe producing a stable gel in water (Fig. 3i–j), suggesting that GOVM-gel has good injectability.

Indeed, it is widely acknowledged that hydrogels are subject to mechanical forces when applied to damaged tissues, which can cause degradation, limiting their lifespan and changing their function [50]. Their remarkable self-healing property suggests that hydrogels can adjust to external mechanical strain [52]. Accordingly, we evaluated the self-healing capacity of GOVM-gel at  $37\text{ }^\circ\text{C}$  (Fig. 3k). These results demonstrate that GOVM-gel is subject to a quick sol-gel transition following external stress, corroborating that it has exceptional self-healing properties.

Finally, the antibiotic release curve and electron microscopy were

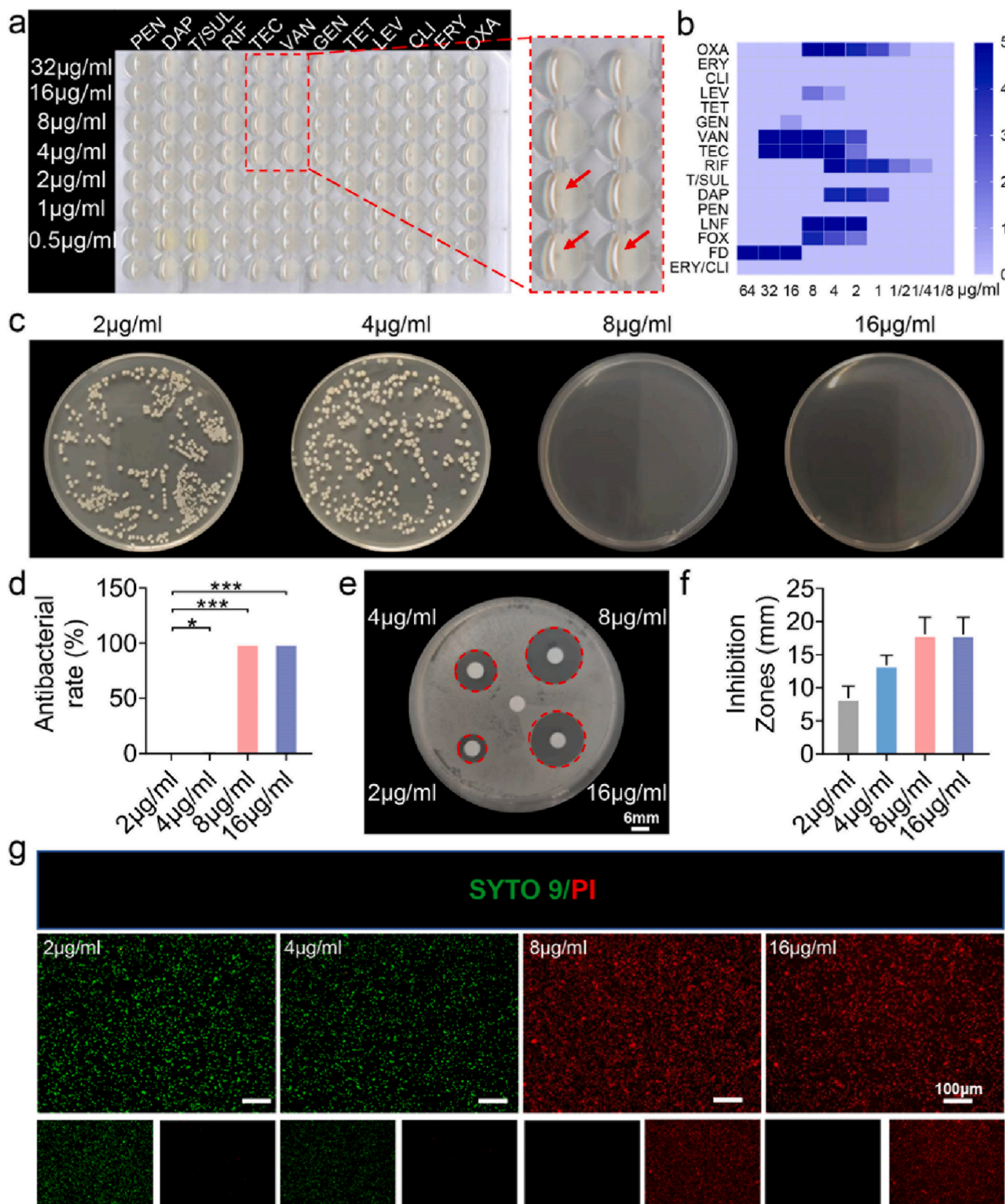


**Fig. 2.** Screening for drug susceptibility of *Staphylococcus aureus*. (a) Drug-sensitive plate screening for antibiotics sensitive to *Staphylococcus aureus*. (b) Heat map analysis of drug susceptibility screening results. (c) Agar plate was coated to detect the bactericidal concentration of antibiotics. (d) Quantitative analysis of the antibacterial rate. (e) Bacteriostatic zones produced by different concentrations of antibiotics. (f) Quantitative analysis of the inhibition zones. (g) Bacteria live/dead staining ( $n = 3$ ,  $*p < 0.05$ ,  $**p < 0.01$ , and  $***p < 0.001$ ).

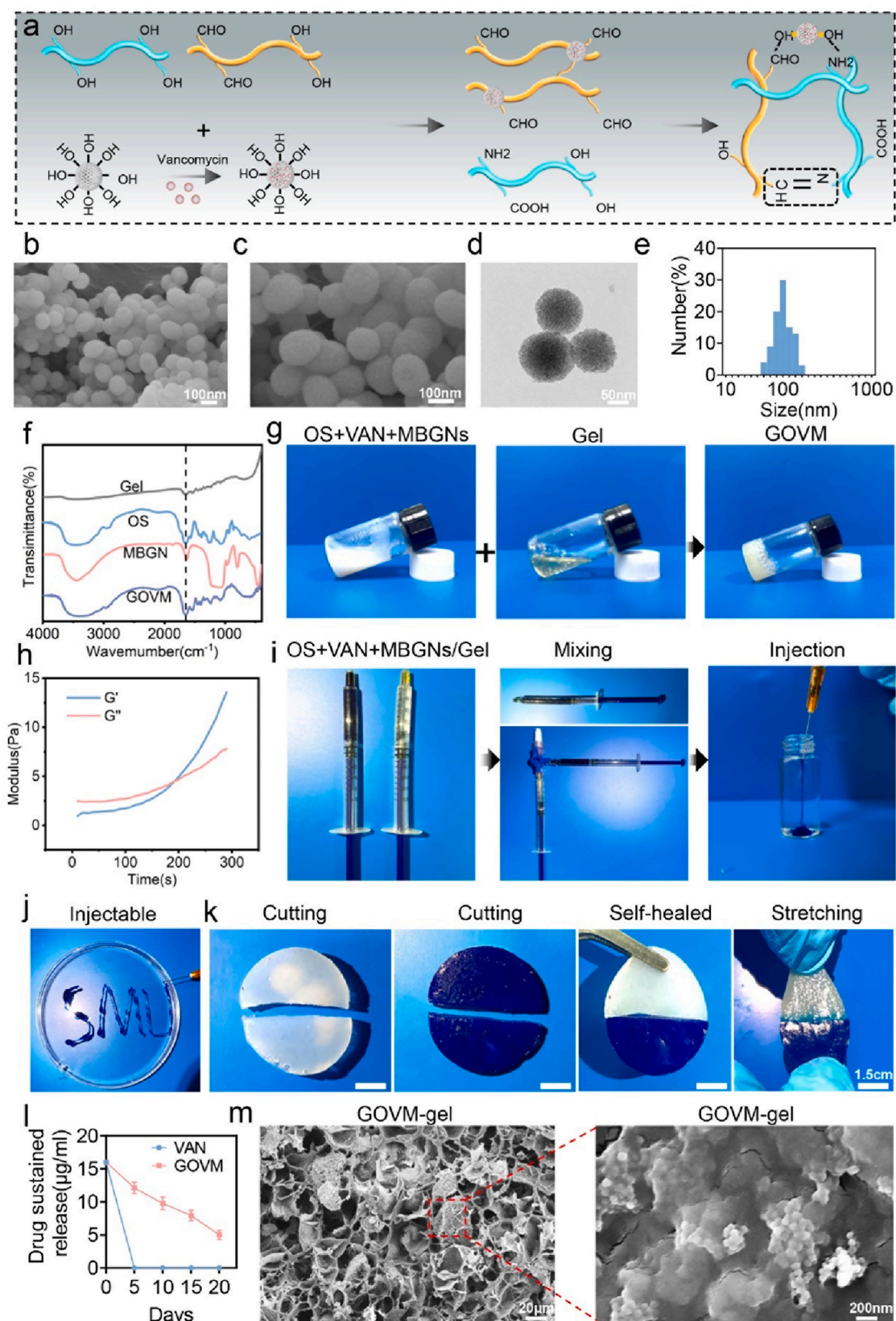


**Fig. 3.** Characterization of GOVM-gel. (a) Diagram of the synthesis of GOVM-gel. (b–c) Scanning electron microscope (SEM) images of mesoporous bioactive glass nanoparticles (MBGNs). (d) Transmission electron microscope (TEM) images of MBGNs. (e) Average hydrodynamic size of MBGNs. (f) FTIR spectra of GOVM-gel. (g) Photographs show the mixing of gelatin (30% (w/v)) and OS (10% (w/v)) containing MBGNs (5% (w/v)) to form GOVM-gel in a glass bottle at 37 °C. (h) Dynamic time sweep rheological analysis to assess gelation kinetics of GOVM-gel. (i–j) Injectability of GOVM-gel. (k) Demonstration of the self-healing capacity by cutting gelled GOVM-gel into halves and rejoining them to obtain healed interfaces. (l) Sustained release curve of VAN in vitro. (m) Scanning electron microscope (SEM) images of GOVM-gel.

used to evaluate the successful preparation of GOVM-gel. The cumulative release curve of VAN indicates the effective release of the drug from the adhesive (Fig. S5), and the antibiotic sustained-release curve revealed the substance's sustained bactericidal activity (Fig. 3I). Compared with conventional antibiotics, the local antibiotic concentration of GOVM-gel was above the minimum inhibitory concentration after 15 days. The morphology of GOVM-gel was then examined using SEM. As shown in Fig. 3m, GOVM-gel had a normal porous structure and a rough surface (Fig. S6). The pore surfaces were relatively rough due to the adhesion of MBGNs, which provides a 3D environment for cell adhesion, ingrowth, and proliferation [37], determining cell behavior. Overall, these findings indicate that GOVM-gel was effectively manufactured.

### 3.3. *Ex vivo* adhesiveness characterization with porcine bone

A fresh cancellous bone fragment from pig ribs was used to assess the adhesion strength and flexibility of GOVM-gel adhesives. Bone fragments were joined end-to-end and lap-to-shear using the three types of GOVM-gel adhesives (Fig. 4a–b). Given that the biological environment is mimicked by preconditioning the bone fragments in PBS solution at 37 °C, biomechanical testing was performed on the attached bone fragments. Experimental results showed that the bone adhesive without MBGNs had the lowest adhesive strength before adhesion breakdown (Fig. 4c–d). During lap-shear testing, the GOVM-gel demonstrated superior adhesive strength above 315.19 kPa. On the other hand, the incorporation of 3% MBGNs significantly improved the adhesive strength, which could be further refined by adjusting the content to 5% (w/v) ( $325.05 \pm 7.17$  kPa for end-to-end,  $315.94 \pm 8.51$  kPa for lap-shear) (Fig. 4c–d). In contrast, adding MBGNs could slightly decrease the adhesion strength, with no significant changes observed after increasing the MBGNs content up to 7% (w/v), suggesting a change in the equilibrium between the cohesiveness and adhesion of the GOVM-gel adhesive, which may be attributed to the cohesive or adhesive failure of the glue itself or a mixture of causes, indicating failure of the adhesive-tissue interface [14]. We hypothesized that the inferior mechanical strength of the GOV adhesive might be attributed to its low cohesion. Although adding MBGNs might increase the cohesiveness of the adhesive, it could also consume the aldehyde groups responsible for the adhesiveness [53]. Consequently, when the MBGNs concentration was increased to 7% w/v, in addition to a modest increase in cohesiveness, an overdose of MBGNs could deplete aldehyde groups, resulting in a decline in the adhesiveness of the GOVM-gel, characterized by the decrease in adhesive strength. Taking into account both the cohesiveness and adhesion of the material, we inferred that GOVM-gel reinforced with 5% w/v MBGNs exhibited an optimal performance. We demonstrated the strength of the improved formula by affixing a newly sawn bone fragment to pig femur and utilizing the attached joint to hoist a container containing 2.69 L of deionized water (Fig. 4e–f). With an adhesion area of 8.50 cm<sup>2</sup>, the raised water container indicated an adhesive strength of 31.65 kPa, demonstrating good adhesion properties. The tissue adhesive properties of GOVM-gel originate from the formation of chemical/physical bonds between the GOVM-gel and tissue. First, the cohesion of the hydrogel is provided by the dynamic Schiff base bond and hydrogen bond formed between OS and Gel. Meanwhile, MBGNs as connectors can achieve a high adhesion strength between hydrogels and surrounding tissues. And the MBGNs as cross-linkers enable the hydrogel network to be significantly enhanced.

In addition to adhesive strength, appropriate flexibility while exerting adhesiveness has significant value. Properties such as flexibility and adjustable adhesiveness help the surgeon to fuse the bone fragment [54,55] since many modifications are often required to achieve a satisfactory reduction. Our GOVM-gel displayed good adhesive flexibility when adhering to bone fragments. We demonstrated such flexibility by disassembling and reassembling two pairs of bound bone fragments after exchanging one bone fragment between the two pairs

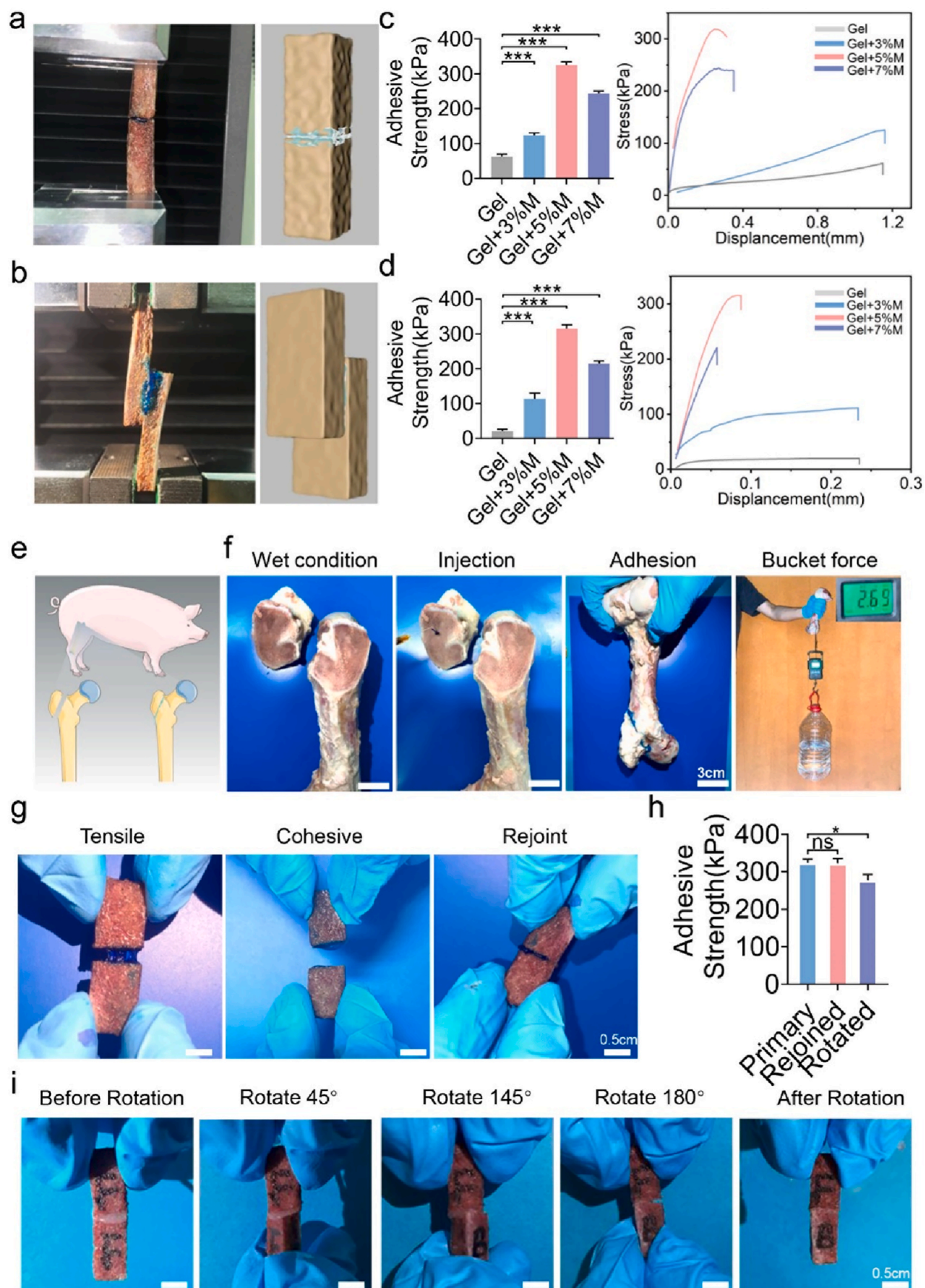
(Fig. 4g). The reunited portions exhibited immediate re-adhesion with a distinct boundary at the rejoined interface, which became unclear when the adhesives on the interface self-healed. Moreover, the adhesive strength of the reunited bone fragments was evaluated after preconditioning. The rejoined and healed bone fragments treated with GOVM-gel to bone fragments revealed comparable strength (Fig. 4h). In addition, the flexibility was demonstrated by rotating one of a connected pair of bone fragments by 180° (Fig. 4i). Initial adhesion of the pair was maintained following rotation and self-healing; however, the connected bone pieces exhibited decreased strength compared to the non-rotated pair (Fig. 4h). Indeed, the reversible adhesion of GOVM-gel connected pieces is essential to allow surgeons to conduct simple modification during splicing procedures [14]. Interestingly, the GOVM-gel could successfully fill the spaces between fragments and finally mend the open fracture fragments.

### 3.4. *In vitro* antibacterial properties of GOVM-gel

Infection is one of the most serious complications of open fractures and is a major obstacle to wound healing [5]. Importantly, biomaterials with antibacterial properties may prevent pathogenic bacteria spread and improve wound healing in an open fracture [56,57]. To this end, surface antibacterial activity tests were conducted to assess the antibacterial properties of the GOVM-gel against *S. aureus* [58]. Following treatment with the hydrogels at 37 °C, most *S. aureus* (~99.90%) were inactivated by these hydrogels at 24 h, corroborating the antibacterial efficacy against *S. aureus*, while the antibiotic alone group and hydrogel with the antibiotic group showed almost no bacteria colonies compared with the PBS-treated control and GOM groups (Fig. 5a). Further quantitative study revealed good antibacterial efficacy of the GOVM-gel (Fig. 5b). We further substantiated the bacteriostatic effect of the material by quantifying the size of the inhibition zone. We found that the bacteriostatic region of the GOVM group was much larger than the VAN group (Fig. 5c). In this respect, the bacteriostatic area of the GOVM group was 16 mm, which was two-fold that of the VAN group (Fig. 5d), and the GOVM group exhibited better bacteriostatic effects than the VAN group, which may be related to the sustained release effect of antibiotics in the material. Meanwhile, the bactericidal effect was verified by counting bacteria in each group (Fig. 5e). The antibacterial properties against *S. aureus* were also evaluated through bacteria live/dead staining to determine whether the adhesive could provide an appropriate antibacterial effect (Fig. 5f). The results showed more significant bacterial death (red fluorescence) in the GOVM-gel group and the VAN group compared with the PBS group and the GOM group, which was validated by quantitative analysis (Fig. 5g), indicating effective antibacterial efficacy of the GOVM-gel. The enhanced antibacterial effect was attributed to the destruction of the bacterial cell wall by antibiotics themselves, while the special mesh structure provided by hydrogels allowed the sustained release of drugs and maintained the antibacterial concentration for a long time [59].

### 3.5. *In vitro* biocompatibility and bioactivity of GOVM-gel

Biocompatibility is essential for the clinical application of materials in human tissues and organs [60]. Since bone adhesives are in direct contact with the adhered body's tissue, we further evaluated their biocompatibility. First, we cultured BMSCs on the surface of the hydrogel material to examine their toxic effects on cells. Live/dead staining was performed after 24 h of culture to determine the viability of the cells (Fig. 6a). Significant green fluorescence was observed on the surface of the hydrogel, indicating that most cells survived. The red fluorescence, which represents dead cells, was barely visible. At the same time, the fluorescence-based quantitative analysis showed comparable findings between the experimental and the control groups (Fig. 6b). Our findings suggest that the GOVM-gel did not significantly reduce the abundance of living cells compared to the control group,



(caption on next page)

**Fig. 4.** Characterization of GOVM-gel strength and reversible adhesiveness by fresh porcine bone samples. (a) End-to-end GOVM-gel strength test. (b) Lap-shear GOVM-gel strength test. (c) Representative stress-displacement curve and adhesive strength of end-to-end tensile test after incorporating different ratios of MBGNs. (d) Lap-shear adhesive strength of GOVM-gel after incorporation of MBGNs and its representative stress-displacement curve. (e) Schematic diagram of bone glue bonding pig femoral head. (f) Demonstration of the adhesive strength of glued bone piece from porcine femur using GOVM-gel by lifting a bucket containing 2.69L water. (g) Demonstration of the reversible adhesiveness through rejoining bone pieces with residual GOVM-gel after the failure of the glued joint. (h) Comparative study GOVM-gel adhesives on the primary adhesive strength before failure and secondary adhesive strength after rejoining. (i) Demonstration of the adjustable adhesiveness via rotating one of the bone pieces for 180° after binding them with GOVM-gel. (n = 3, \*p < 0.05, \*\*p < 0.01, and \*\*\*p < 0.001).

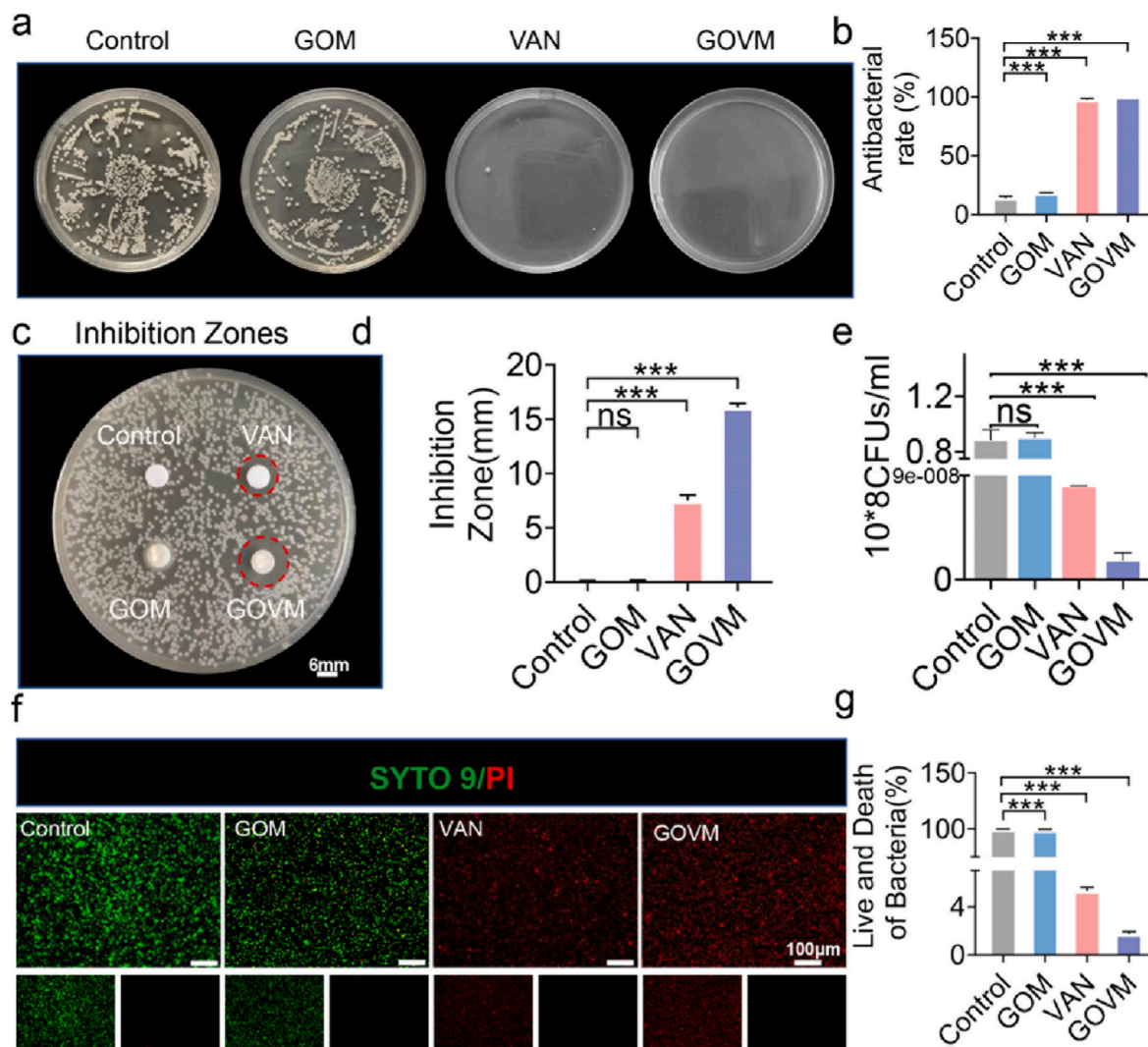


**Fig. 5.** Antibacterial properties of GOVM-gel. (a) Images of bacterial colonies on the agar plates after contact with different hydrogels. (b) Quantitative analysis of the number of colonies. (c) Inhibition zones size of different groups. (d) Quantitative analysis of the inhibition zones. (e) Bacteriostatic effect of the hydrogel and its quantitative analysis. (f–g) Bacteria live/dead staining and its quantitative analysis (n = 3, \*p < 0.05, \*\*p < 0.01, and \*\*\*p < 0.001).

highlighting that the bone adhesive was biocompatible. In addition, we cultured the cells on the hydrogel for 48 h and uniform spreading of cells was observed on the hydrogel surface (Fig. 6c), indicating the healthy state of the cells. Quantitative analysis showed no significant difference in the cell spreading area on the hydrogels compared with the control group (Fig. 6d), which indicates the good biocompatibility of GOVM-gel. Moreover, BMSCs proliferation on the hydrogel was quantified by the CCK-8 assay (Fig. 6e). There was no difference in OD value between the GOVM and control groups, and the GOVM-gel did not impact BMSCs proliferation.

### 3.6. In vivo biocompatibility and bioactivity of GOVM-gel

The safety of materials in vivo is the premise and basis of tissue

engineering applications [61]. To further evaluate GOVM-gel biocompatibility in vivo, blood was collected from the rat inferior vena cava for hemolysis test and biochemistry studies, and the major organs, including the heart, liver, spleen, lung and kidney tissues were harvested for histopathological analysis. There was almost no hemolysis in the GOVM group and PBS group (Fig. 6f), as hemolysis levels were lower than the normal range (5%) (Fig. 6g) [62]. HE staining showed that the hydrogel yielded no significant damage to organs and tissues, proving that it had no toxic effect (Fig. 6h). In addition, as shown in Fig. 6i, in the control group and GOVM groups, liver and kidney function were not affected as measured by alanine aminotransferase (ALT), aspartate aminotransferase (AST), alkaline phosphatase (ALP), or blood creatinine (CR). Meanwhile, the white blood cell (WBC) count, red blood cell (RBC) count, red cell distribution width (RDW), and platelet (PLT) count in rat

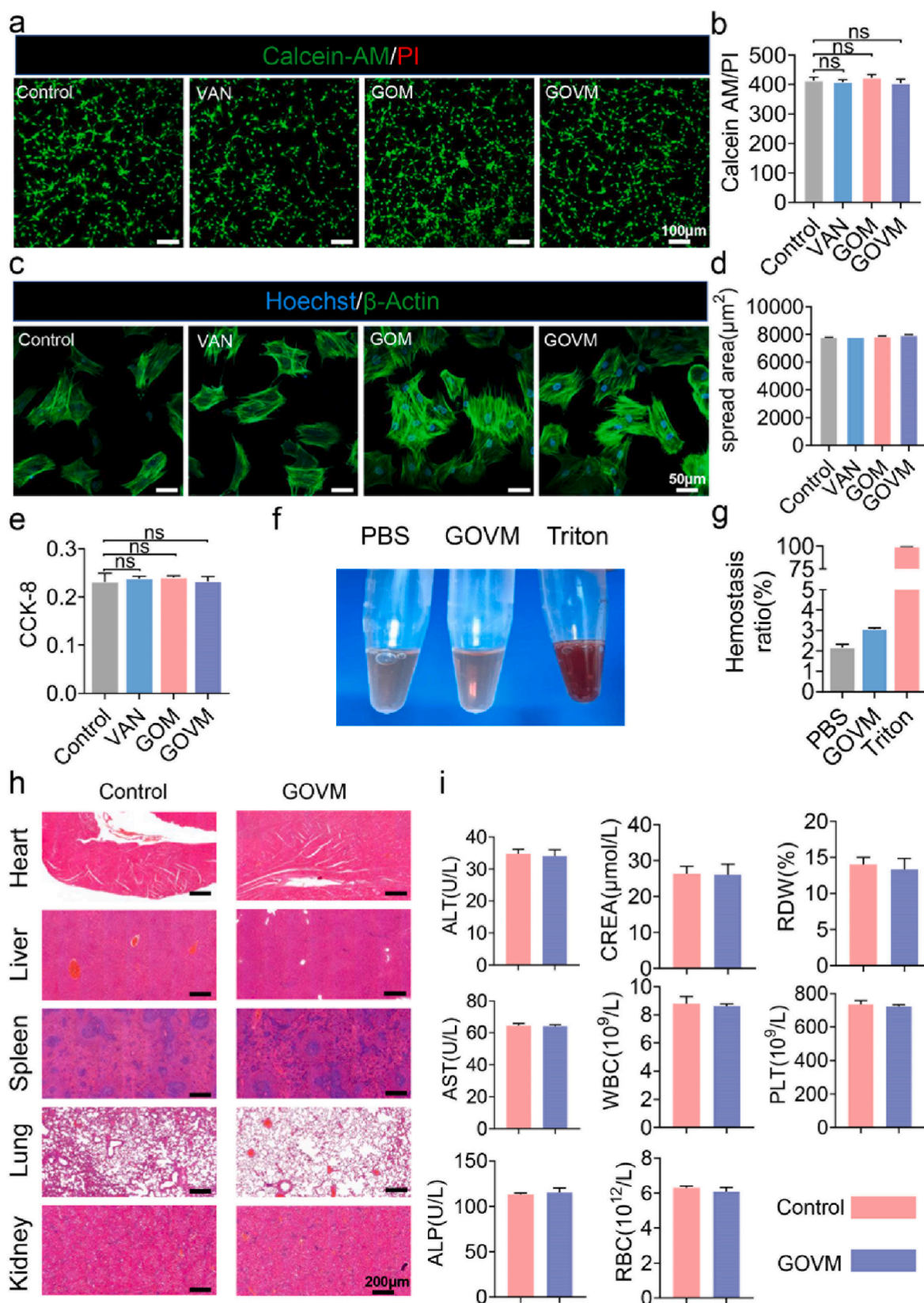


**Fig. 6.** Biocompatibility of GOVM-gel. (a) The live/dead staining of BMSCs after 24 h co-culture with different hydrogels, live cells are marked with green fluorescence, and dead cells are marked with red fluorescence. (b) Quantitative analysis of the live dead staining. (c) Cytoskeleton staining photos of cells cultured on the hydrogel after 48 h. (d) Quantitative analysis of the cell spreading area. (e) CCK-8 assay results of BMSCs cultured on the hydrogels after 2 days. (f) Hemolysis test of materials. (g) Quantitative analysis of Hemolysis test. (h) The pathological examinations of the heart, liver, kidney and lung of mice in control and GOVM-gel groups. (i) Serum levels of biomarkers reflecting liver function and kidney function, and the parameters of blood cells in rat by GOVM-gel ( $n = 3$ , \* $p < 0.05$ , \*\* $p < 0.01$ , and \*\*\* $p < 0.001$ ).

blood were within the normal range, suggesting no hematologic toxicity. Overall, these results indicate the high biocompatibility of the GOVM-gel.

### 3.7. Degradation of GOVM-gel in vitro and in vivo

The biodegradability of biomaterials implanted in the body is also of great significance. Hence, we further assessed the biodegradation of GOVM-gel. As shown in Fig. 7a, the degradation of GOVM-gel in vitro was initially rapid and then slowed down. In this respect, the degradation rate was fast for the first 10 days, and the mass of the residual adhesive decreased to 49.4%. After that, the degradation rate slowed down and was completely degraded after 20 days. Most of the degradation products were starch, gelatin monomer, and bioactive glass, and the gradual dissolution of hydrogel induced the weight loss from the outside to the inside rather than by the mechanical agitation of the gel (Fig. S7). To evaluate the degradation of hydrogels in vivo, the adhesive with Cy7.0 fluorescence was injected subcutaneously and into the skull fracture site of rats (Fig. 7b–f). In vivo imaging showed a gradually declining fluorescence signal of hydrogel Cy7.0, which was no longer observed after 20 days. In addition, we made general observations on the implanted hydrogels at the indicated time points. Importantly, none of the tissue around the experimental site showed signs of inflammatory reactions such as swelling or redness throughout the implantation process (Fig. 7g), consistent with our previous research [63]. As expected, the adhesive bulk also gradually decreased with a subtle amount of residual on day 20. Overall, these results confirm that GOVM-gel exhibits a good biodegradation performance.

### 3.8. GOVM-gel enhances osteogenic differentiation of BMSCs

To further assess the osteogenic ability of GOVM-gel on BMSCs, cells

were treated with the hydrogel for 7 and 14 days, respectively. Early detection of the osteogenic marker ALP showed a higher amount of blue precipitate in the GOM and GOVM groups than in the control group (Fig. 8a), which highlights the pro-osteogenic activity of the GOVM-gel on BMSCs. ARS was used as a late indicator of osteogenic differentiation. On day 14, we found a large number of red calcium nodules were precipitated in the experimental group compared with the control group (Fig. 8b). At last, the GOM and GOVM groups exhibited higher values than the control group during quantitative analysis (Fig. 8c–d). Current evidence suggests that MBGNs confer osteogenic effects to BMSCs [37], the bone formation processes involve the release of ions from dissolved products and induce biotin precipitation [32]. Our experimental results can further account for the enhanced osteogenic ability of cells in GOM and GOVM groups.

In addition, to assess the effect of the bone adhesive on the levels of osteogenic genes, OPN and RunX2 were used to investigate osteogenic differentiation [37]. The expression of all osteogenic genes was up-regulated in GOM and GOVM groups by RT-PCR after 14 days of BMSCs cultured on a conditioned medium (Fig. 8e–f). The immunofluorescence assay results indicated that compared with the control group, the fluorescent intensity in the experimental group was enhanced (Fig. 8g), and quantitative analysis further validated the difference between both groups (Fig. 8h). Consistently, Western blot showed that the GOM and the GOVM groups yielded higher protein expression of RunX2 and OPN than the control group (Fig. 8i). Moreover, the GOM group and the GOVM-gel group yielded significant differences with the control group (Fig. 8j). These results suggest that the GOVM-gel can promote BMSCs osteogenic differentiation, and MBGNs plays an important role in the osteogenic differentiation of BMSCs [64], and can indirectly promote bone formation and regeneration by regulating inflammation [65,66]. Furthermore, it can be used clinically to make orthopedic stents and drug delivery systems [67]. In a nutshell, this bone adhesive with

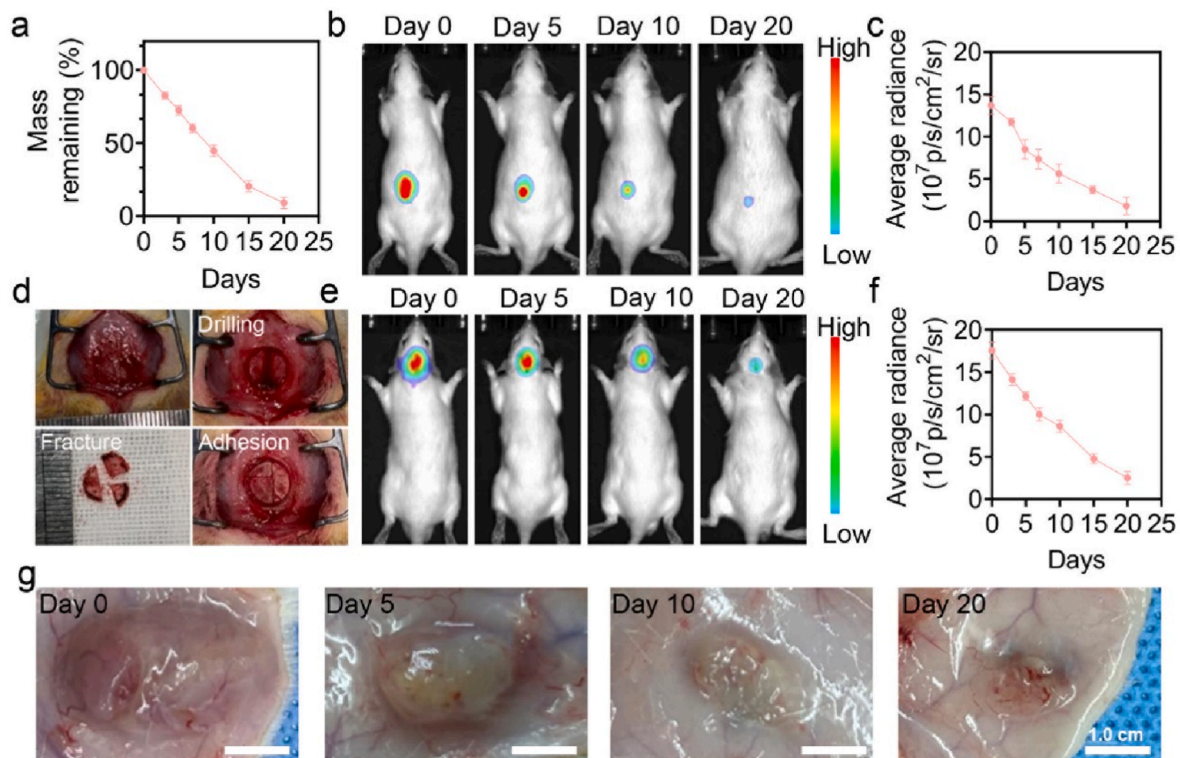


**Fig. 7.** Biodegradation of GOVM-gel. (a) The remaining weight of GOVM-gel (%) during incubation in PBS. (b–c) The fluorescence AURA imaging for the in vivo subcutaneous degradation of Cy7.0-labelled GOVM-gel and its quantitative analysis. (d) Adhesion diagram of adhesive in rat skull open fracture model. (e–f) The fluorescence AURA imaging for the in vivo cranial degradation of Cy7.0-labelled GOVM-gel and its quantitative analysis. (g) General observation of subcutaneous degradation of GOVM-gel ( $n = 3$ , \* $p < 0.05$ , \*\* $p < 0.01$ , and \*\*\* $p < 0.001$ ).

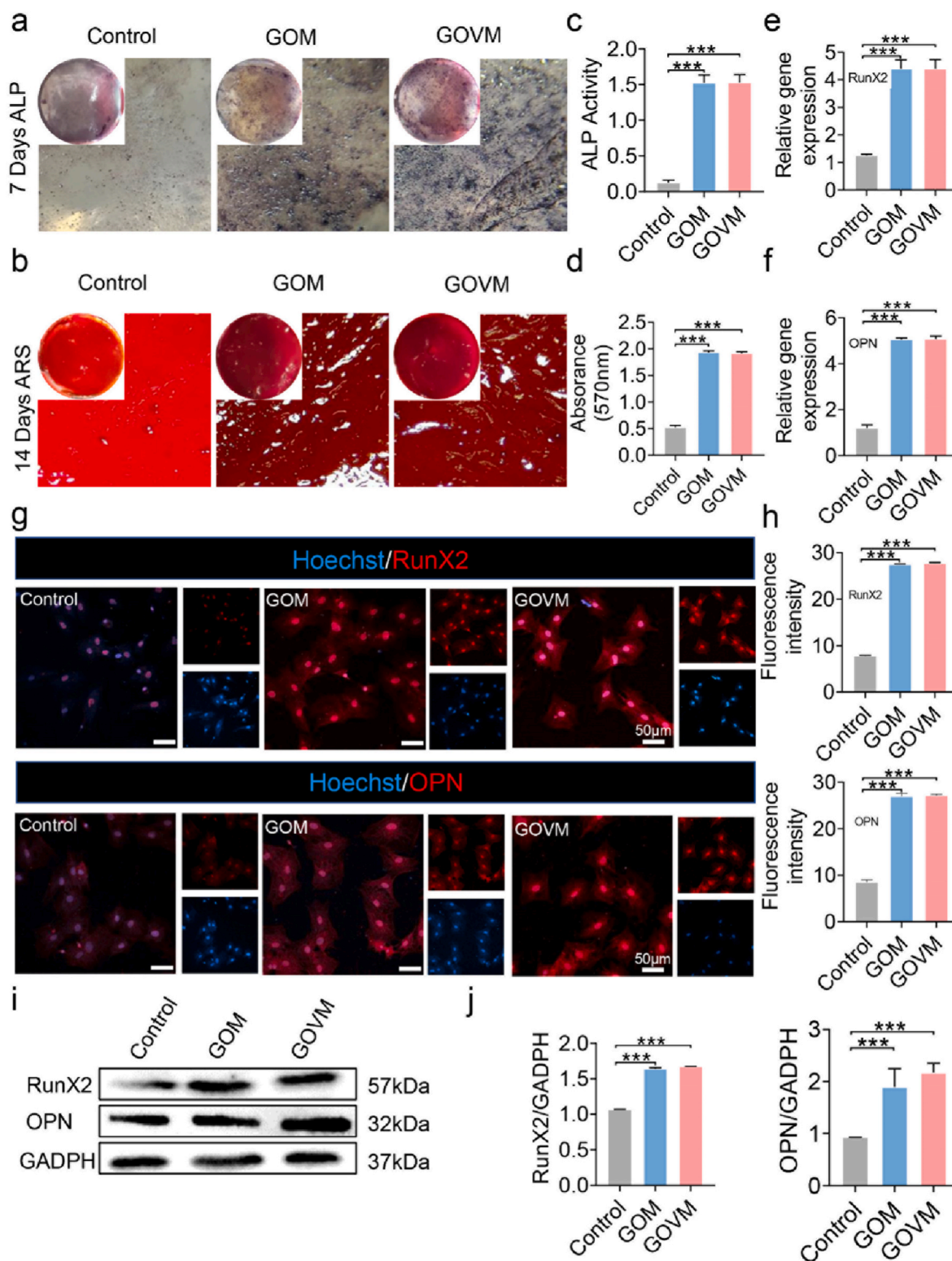


**Fig. 8.** In vitro ALP expression and calcium biomaterialization of BMSCs cultured on the hydrogels. (a) ALP staining of BMSCs on day 7 and Alizarin red S staining on day 14. (b) Alizarin Red S staining mineral layer. (c) Quantitative ALP activity of BMSCs. (d) Quantitative ARS activity of BMSCs. (e–f) RT-PCR analysis of osteogenic-related genes encoding OPN and RunX2. (g–h) Representative immunofluorescent images of osteogenic-associated proteins RunX2 and OPN in different groups. RunX2 and OPN are marked by red fluorescence, and the cell nuclei were dyed blue by Hoechst. (i) Protein expression of OPN and RunX2 in BMSCs with GAPDH as a reference. (j) Quantitative RunX2 and OPN Protein expression (n = 3, \*p < 0.05, \*\*p < 0.01, and \*\*\*p < 0.001).

bioactive glass can be used for bone regeneration-related applications.

### 3.9. In vivo antibacterial properties of GOVM-gel

Clinically, refractory infections after an open fracture have become a major conundrum in the medical field, posing a serious threat to human health and survival [56]. Indeed, orthopedic implants with antimicrobial effects can effectively reduce the infection of pathogenic bacteria caused by open fractures [68]. We further evaluated the in vivo antimicrobial properties of the GOVM-gel using a subcutaneous abscess model induced by *S. aureus* infection (Fig. 9a) [69–71]. In this respect, subcutaneous abscesses were formed one week after *S. aureus* subcutaneous injection (200  $\mu$ L,  $10^8$  cfu/mL). HE staining showed significant infiltration of a large number of inflammatory cells in the control and GOM groups and a large number of *S. aureus* bacteria were observed in the infected tissue site by Giemsa staining (the red arrows indicate bacteria) (Fig. 9b). However, the VAN group and the GOVM group exhibited decreased bacterial abundance than the two groups. The above results suggest that the antibacterial GOVM has huge prospects for application as implants to enhance the healing of infected wounds.

### 3.10. GOVM-gel promotes bone regeneration in vivo

To assess the in vivo bone regeneration ability, the hydrogel was injected into the defect site of skull fracture in situ after establishing an open skull fracture model in rats (Fig. 10a) [72]. Six weeks later, the skull underwent a micro-CT scan and HE and immunohistochemical staining. Micro-CT results showed the growth of new autologous bone tissue at the edge of the skull critical defect in GOM and GOVM groups compared with the control group (Fig. 10b). Sagittal and coronal images further confirmed the continuous regeneration of bone formation in the defect. Quantitative micro-CT analysis revealed that the GOVM group demonstrated a significantly higher amount of bone volume regenerated (Fig. 10c) and thicker trabecular bone than the control group. Moreover, it was found that MBGNs containing GOM and GOVM exhibited significantly better bone regeneration capacity than the control group. Accordingly, GOM and GOVM may facilitate faster and more efficient healing of bone defects.

In addition, Masson's trichrome and HE analyses confirmed that bone regeneration was facilitated by the GOVM-gel. After 6 weeks, HE and Masson staining showed that the bone mass around the fracture was significantly increased in the GOM and GOVM groups, and fully mature

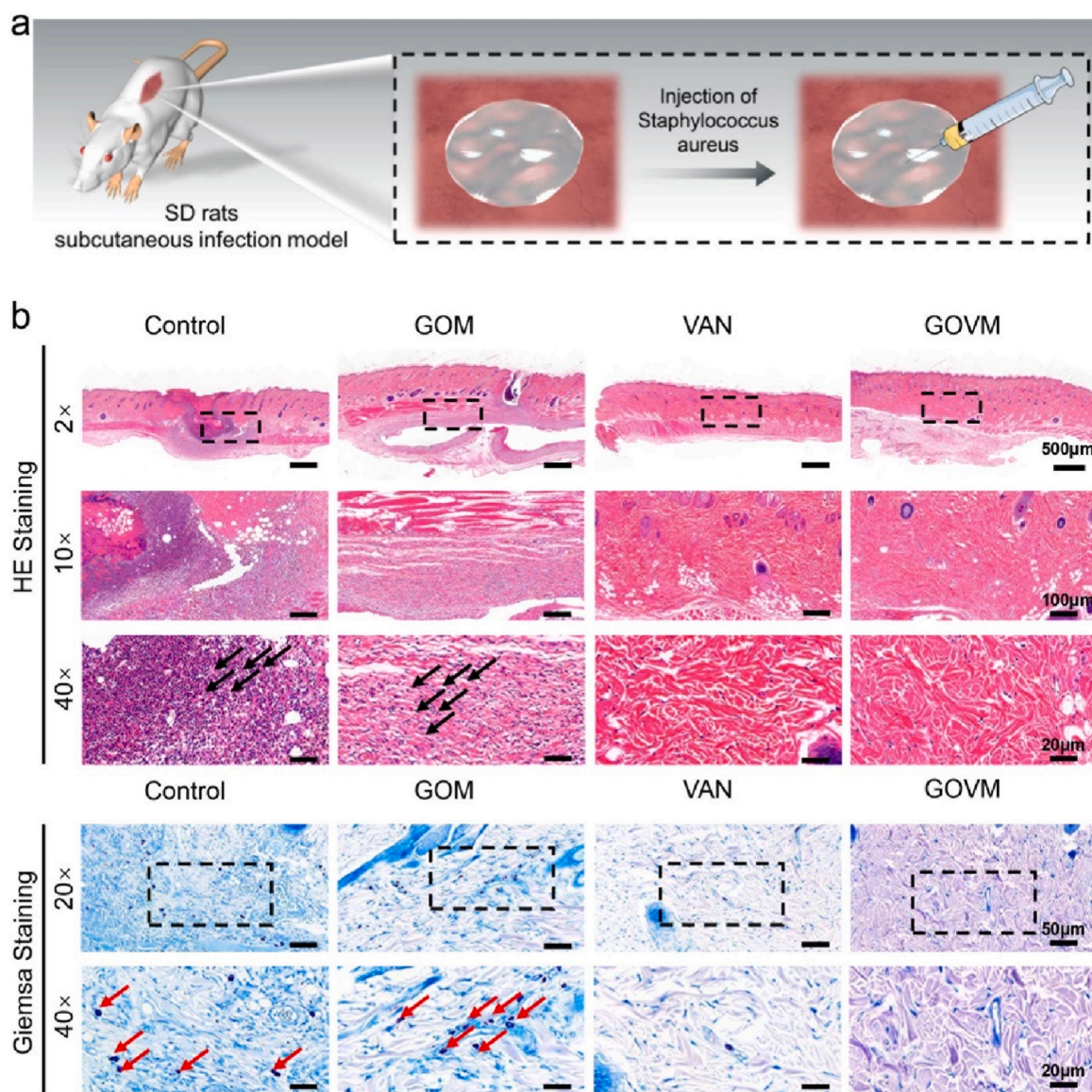
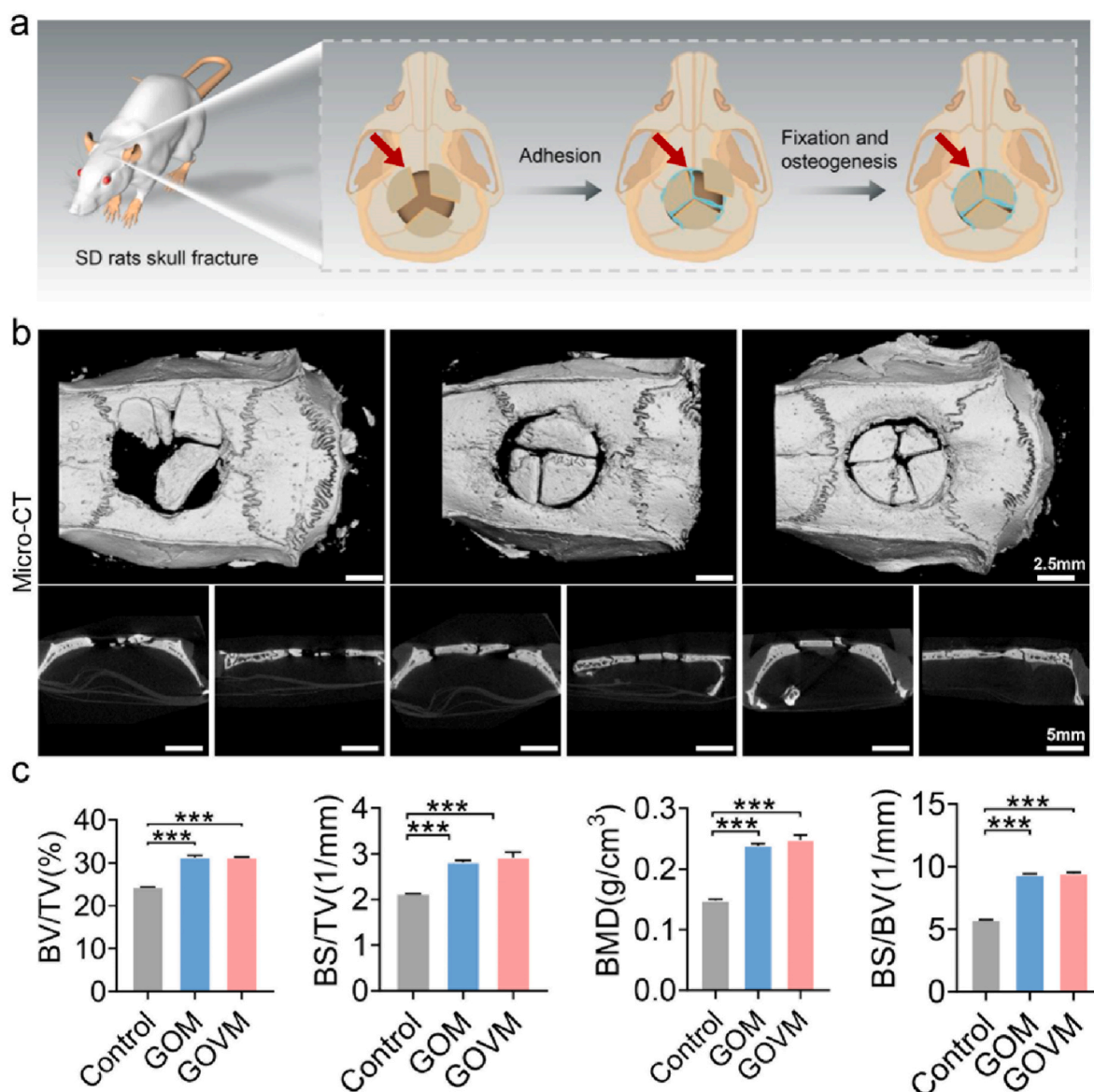


Fig. 9. Antibacterial properties of GOVM-gel in vivo. (a) Schematic diagram of a subcutaneous abscess in a rat. (b) HE and Giemsa staining with different hydrogels.



**Fig. 10.** In vivo bone regeneration after 6 weeks of implantation of the bone hydrogels. (a) Schematic of skull fracture in rats. (b) Micro-CT images of open fracture cranial defects in rats. (c) Quantitative analysis of bone volume and trabecular thickness ( $n = 3$ , \* $p < 0.05$ , \*\* $p < 0.01$ , and \*\*\* $p < 0.001$ ).

bone tissue could be observed (Fig. 11a). However, only a small amount of regenerating new bone tissue was observed in the control group, with less bone formation near the original defect, and poor osseous closure.

Immunohistochemical staining showed upregulation of osteogenesis-related genes OPN and RunX2 expression in rat tissues (Fig. 11b). Quantitative analysis showed that the GOM and GOVM groups had higher expression levels than the control group (Fig. 11c). Based on the imaging and histological results, compared with the control group, the regeneration of bone tissue was effectively enhanced in the GOM and GOVM groups, with the repair of tissue defects and osteogenic properties in vivo.

The above results indicate that MBGNs could effectively promote osteogenesis. On the one hand, MBGNs could stimulate the proliferation of bone cells through apatite crystallization and ion release on the material surface, thus forming new bone. On the other hand, the degradation of MBGNs played an important role in regulating the growth of bone cells by forming an acid-base microenvironment at the interface between materials and tissues. Our in vitro osteogenic experiments yielded consistent results, suggesting MBGNs provide a good therapeutic approach to promote bone formation for open fractures. Overall, the

GOVM-gel has huge prospects for application during clinical practice to promote bone regeneration in orthopedics.

#### 4. Conclusion

In this study, we developed an antibacterial and osteoconductive adhesive as a treatment tool to promote the reduction of open fractures and guide subsequent bone regeneration and antibacterial activity. The in vitro adhesion experiment of porcine bone proved that the GOVM-gel could adhere to fracture fragments of open fracture, given its high flexibility, injectability, fit-to-shape capacity, and reversible adhesiveness. At the same time, the results of in vitro antibacterial, osteogenic gene and protein expression experiments (OPN, RunX2) showed that GOVM-gel exhibited good antibacterial effects and promoted new bone formation. More importantly, in the in vivo rat subcutaneous infection model and open skull fracture model, the GOVM-gel yielded antibacterial effects and enhanced bone regeneration. Taken together, the GOVM-gel exhibited huge potential as an excellent biomaterial for bone fixation, regeneration, repair and anti-infection during open fracture. Nonetheless, further studies are warranted before clinical application.

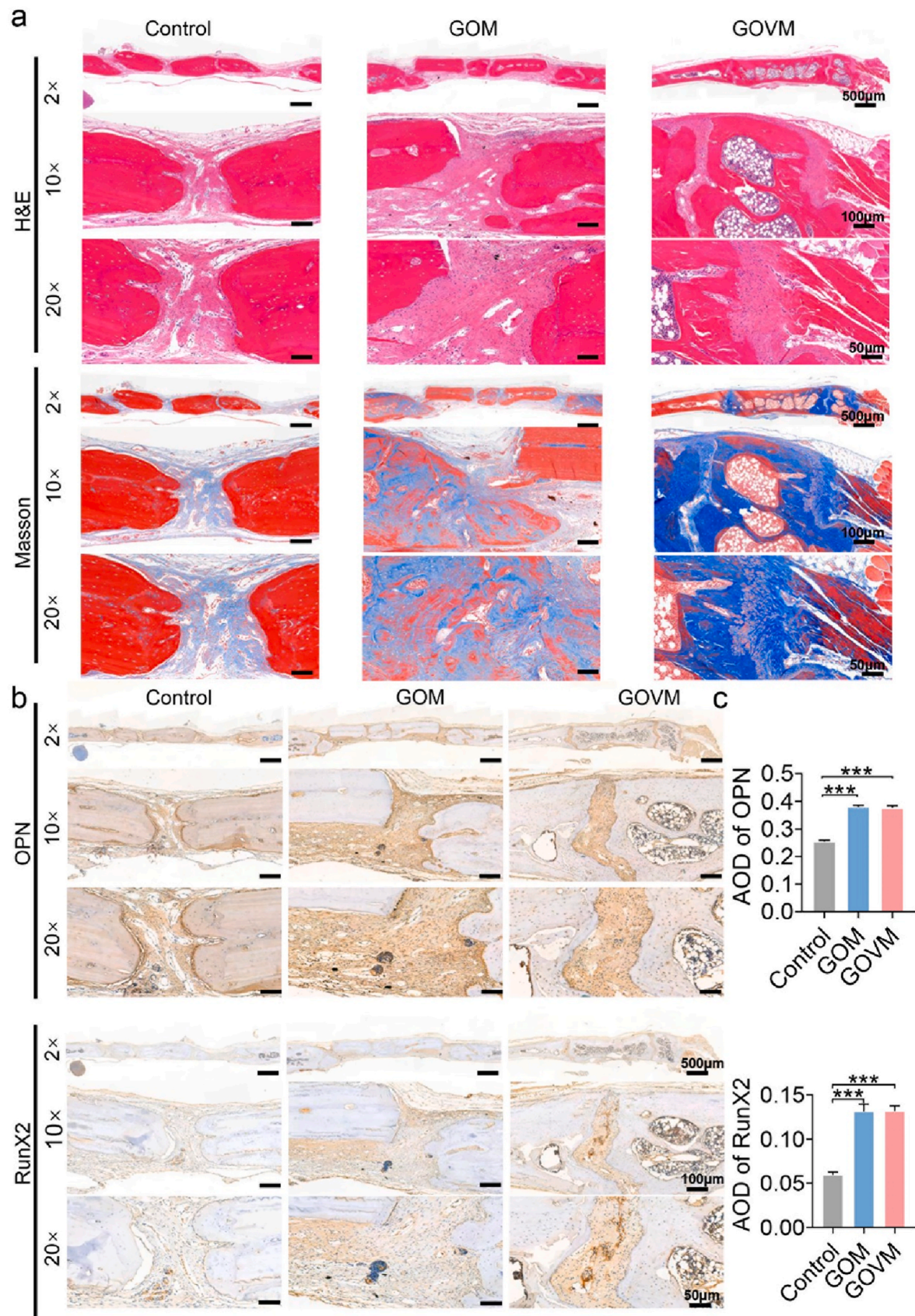


**Fig. 11.** In vivo bone regeneration after 6 weeks of implantation of the bone hydrogels. (a) H&E and Masson's trichrome staining of histological sections of calvarial decalcified sections after hydrogel implantation. (b) Immunohistochemical staining of skull tissue. (c) Quantitative analysis of immunohistochemical staining (n = 3, \*p < 0.05, \*\*p < 0.01, and \*\*\*p < 0.001).

## Ethics approval and consent to participate

All animal experiments were carried out in the Animal Experimental Center of Nanfang Hospital. All operations were trained, and the experimental protocol was reviewed and approved by the Ethics Committee of Southern Medical University.

## CRediT authorship contribution statement

**Yusheng Yang:** Conceptualization, Methodology, Formal analysis, Validation, Investigation, Writing – original draft. **Shenghui Su:** Methodology, Validation, Formal analysis. **Shencai Liu:** Methodology, Validation, Formal analysis. **Weilu Liu:** Methodology, Formal analysis, Validation. **Qinfeng Yang:** Visualization, Investigation. **Liangjie Tian:** Methodology. **Zilin Tan:** Methodology. **Lei Fan:** Formal analysis, Funding acquisition, Visualization. **Bin Yu:** Resources, Visualization, Funding acquisition, Data. **Jian Wang:** Methodology, Funding acquisition, Supervision. **Yanjun Hu:** Conceptualization, Methodology, Funding acquisition, Writing – review & editing, Supervision, Data curation, Project administration.

## Declaration of competing interest

The authors declare that they have no known competing financial interests or personal relationships that could have appeared to influence the work reported in this paper.

## Acknowledgments

This work was supported by the Guangzhou Science and Technology Program Key Projects (No.202002020001); Science and Technology Planning Project of Guangdong Province (No.2020A0505100039); Autonomous region science and technology branch Xinjiang project plan (No.2022E02040); Clinical Key Specialty in Ningde City, Fujian Province.

## Appendix A. Supplementary data

Supplementary data to this article can be found online at <https://doi.org/10.1016/j.bioactmat.2023.01.021>.

## References

- [1] M. Omar, C. Zeckey, C. Krettek, T. Graulich, [Open fractures], *Unfallchirurg* 124 (8) (2021) 651–665.
- [2] K. Kortram, H. Bezstarosti, W.-J. Metsemakers, M.J. Raschke, E.M.M. Van Lieshout, M.H.J. Verhofstad, Risk factors for infectious complications after open fractures; a systematic review and meta-analysis, *Int. Orthop.* 41 (10) (2017) 1965–1982.
- [3] A. Diwan, K.R. Eberlin, R.M. Smith, The principles and practice of open fracture care, *Chin. J. Traumatol.* 21 (4) (2018) 187–192, 2018.
- [4] C.J. Foote, P. Tornetta, A. Reito, K. Al-Hourani, M. Schenker, M. Bosse, C.P. Coles, A. Bozzo, A. Furey, R. Leighton, A reevaluation of the risk of infection based on time to debridement in open fractures: results of the GOLIATH meta-analysis of observational studies and limited trial data, *J Bone Joint Surg Am* 103 (3) (2021) 265–273.
- [5] C.G. Zalavras, Prevention of infection in open fractures, *Infect. Dis. Clin.* 31 (2) (2017) 339–352.
- [6] M.L. Costa, J. Achten, J. Bruce, E. Tutton, S. Petrou, S.E. Lamb, N.R. Parsons, Effect of negative pressure wound therapy vs standard wound management on 12-month disability among adults with severe open fracture of the lower limb: the WOLLF randomized clinical trial, *JAMA* 319 (22) (2018) 2280–2288.
- [7] R.A. Gosselin, I. Roberts, W.J. Gillespie, Antibiotics for preventing infection in open limb fractures, *Cochrane Database Syst. Rev.* 1 (2004) CD003764.
- [8] J.J. Seo, N. Mandakbayar, M.S. Kang, J.-Y. Yoon, N.-H. Lee, J. Ahn, H.-H. Lee, J.-H. Lee, H.-W. Kim, Antibacterial, proangiogenic, and osteopromotive nanoglass paste coordinates regenerative process following bacterial infection in hard tissue, *Biomaterials* 268 (2021), 120593.
- [9] B. Li, K.V. Brown, J.C. Wenke, S.A. Guelcher, Sustained release of vancomycin from polyurethane scaffolds inhibits infection of bone wounds in a rat femoral segmental defect model, *J. Contr. Release* 145 (3) (2010) 221–230.
- [10] W.A. Jiranek, A.D. Hanssen, A.S. Greenwald, Antibiotic-loaded bone cement for infection prophylaxis in total joint replacement, *J Bone Joint Surg Am* 88 (11) (2006) 2487–2500.
- [11] S. Mistry, S. Roy, N.J. Maitra, B. Kundu, A. Chanda, S. Datta, M. Joy, A novel, multi-barrier, drug eluting calcium sulfate/biphasic calcium phosphate biodegradable composite bone cement for treatment of experimental MRSA osteomyelitis in rabbit model, *J. Contr. Release* 239 (2016) 169–181.
- [12] M.Y. Krasko, J. Golenser, A. Nyska, M. Nyska, Y.S. Brin, A.J. Domb, Gentamicin extended release from an injectable polymeric implant, *J. Contr. Release* 117 (1) (2007) 90–96.
- [13] C.-Y. Chen, M.-Y. Shie, A.K.-X. Lee, Y.-T. Chou, C. Chiang, C.-P. Lin, 3D-Printed ginsenoside Rb1-loaded mesoporous calcium silicate/calcium sulfate scaffolds for inflammation inhibition and bone regeneration, *Biomedicines* 9 (8) (2021).
- [14] J.C. Tang, K. Xi, H. Chen, L.J. Wang, D.Y. Li, Y. Xu, T.W. Xin, L. Wu, Y.D. Zhou, J. Bian, Z.W. Cai, H.L. Yang, L.F. Deng, Y. Gu, W.G. Cui, L. Chen, Flexible osteogenic glue as an all-in-one solution to assist fracture fixation and healing, *Adv. Funct. Mater.* 31 (38) (2021).
- [15] F. Liska, A. Voss, F.B. Imhoff, L. Willinger, A.B. Imhoff, Nonunion and delayed union in lateral open wedge distal femoral osteotomies—a legitimate concern? *Int. Orthop.* 42 (1) (2018).
- [16] F. Hou, W. Jiang, Y. Zhang, J. Tang, D. Li, B. Zhao, L. Wang, Y. Gu, W. Cui, L. Chen, Biodegradable dual-crosslinked adhesive glue for fixation and promotion of osteogenesis, *Chem. Eng. J.* 427 (2022).
- [17] S. Demetri, G. Vicenti, M. Carrozzo, D. Bizzoca, D. De Franceschi, B. Moretti, The Masquelet technique in the treatment of a non-infected open complex fracture of the distal tibia with severe bone and soft tissue loss: a case report, *Injury* 49 (Suppl 4) (2018) S58–S62.
- [18] J. Muñoz Vives, J.-C. Bel, A. Capel Agundez, F. Chana Rodríguez, J. Palomo Traver, M. Schultz-Larsen, T. Tosounidis, The floating knee: a review on ipsilateral femoral and tibial fractures, *EFORT Open Rev* 1 (11) (2016) 375–382.
- [19] D.-D. Sun, D. Lv, K. Zhou, J. Chen, L.-L. Gao, M.-L. Sun, External fixator combined with three different fixation methods of fibula for treatment of extra-articular open fractures of distal tibia and fibula: a retrospective study, *BMC Musculoskel. Disord.* 22 (1) (2021) 1.
- [20] M.S. Taljanovic, M.D. Jones, J.T. Ruth, J.B. Benjamin, J.E. Sheppard, T.B. Hunter, Fracture fixation, *Radiographics* 23 (6) (2003) 1569–1590.
- [21] M.J. Parker, H.H.G. Handoll, Extramedullary fixation implants and external fixators for extracapsular hip fractures in adults, *Cochrane Database Syst. Rev.* 1 (2006) CD000339.
- [22] H.H.G. Handoll, J.S. Huntley, R. Madhok, Different methods of external fixation for treating distal radial fractures in adults, *Cochrane Database Syst. Rev.* 1 (2008) CD006522.
- [23] H.H.G. Handoll, J.S. Huntley, R. Madhok, External fixation versus conservative treatment for distal radial fractures in adults, *Cochrane Database Syst. Rev.* 3 (2007) CD006194.
- [24] J. Shao, H. Chang, Y. Zhu, W. Chen, Z. Zheng, H. Zhang, Y. Zhang, Incidence and risk factors for surgical site infection after open reduction and internal fixation of tibial plateau fracture: a systematic review and meta-analysis, *Int. J. Surg.* 41 (2017) 176–182.
- [25] J. Shao, H. Zhang, B. Yin, J. Li, Y. Zhu, Y. Zhang, Risk factors for surgical site infection following operative treatment of ankle fractures: a systematic review and meta-analysis, *Int. J. Surg.* 56 (2018) 124–132.
- [26] J. Huang, X. Jiang, Injectable and degradable pH-responsive hydrogels via spontaneous amino-yne click reaction, *ACS Appl. Mater. Interfaces* 10 (1) (2018) 361–370.
- [27] J.R. Jones, Reprint of: review of bioactive glass: from Hench to hybrids, *Acta Biomater.* 23 (Suppl) (2015) S53–S82.
- [28] S. Naseri, W.C. Lepry, S.N. Nazhat, Bioactive glasses in wound healing: hope or hype? *J. Mater. Chem. B* 5 (31) (2017) 6167–6174.
- [29] K. Zheng, B. Sui, K. Ilyas, A.R. Boccaccini, Porous bioactive glass micro- and nanospheres with controlled morphology: developments, properties and emerging biomedical applications, *Mater. Horiz.* 8 (2) (2021) 300–335.
- [30] H.E. Skallevoid, D. Rokaya, Z. Khurshid, M.S. Zafar, Bioactive glass applications in dentistry, *Int. J. Mol. Sci.* 20 (23) (2019).
- [31] V. Miguez-Pacheco, L.L. Hench, A.R. Boccaccini, Bioactive glasses beyond bone and teeth: emerging applications in contact with soft tissues, *Acta Biomater.* 13 (2015).
- [32] K. Zheng, W. Niu, B. Lei, A.R. Boccaccini, Immunomodulatory bioactive glasses for tissue regeneration, *Acta Biomater.* 133 (2021) 168–186.
- [33] Y. Xu, Y. Zi, J. Lei, X. Mo, Z. Shao, Y. Wu, Y. Tian, D. Li, C. Mu, pH-Responsive nanoparticles based on cholesterol/imidazole modified oxidized-starch for targeted anticancer drug delivery, *Carbohydr. Polym.* 233 (2020), 115858.
- [34] Z. Qiu, B. Zheng, J. Xu, J. Chen, L. Chen, 3D-printing of oxidized starch-based hydrogels with superior hydration properties, *Carbohydr. Polym.* 292 (2022), 119686.
- [35] N.L. Vanier, S.L.M. El Halal, A.R.G. Dias, E. da Rosa Zavareze, Molecular structure, functionality and applications of oxidized starches: a review, *Food Chem.* 221 (2017) 1546–1559.
- [36] K. Zheng, J. Kang, B. Rutkowski, M. Gawęda, J. Zhang, Y. Wang, N. Founier, M. Sitarz, N. Taccardi, A.R. Boccaccini, Toward highly dispersed mesoporous bioactive glass nanoparticles with high Cu concentration using Cu/ascorbic acid complex as precursor, *Front. Chem.* 7 (2019) 497.
- [37] L. Zhou, L. Fan, F.-M. Zhang, Y. Jiang, M. Cai, C. Dai, Y.-A. Luo, L.-J. Tu, Z.-N. Zhou, X.-J. Li, C.-Y. Ning, K. Zheng, A.R. Boccaccini, G.-X. Tan, Hybrid gelatin/oxidized chondroitin sulfate hydrogels incorporating bioactive glass nanoparticles with enhanced mechanical properties, mineralization, and osteogenic differentiation, *Bioact. Mater.* 6 (3) (2021) 890–904.

- [38] Q. Liang, Q. Hu, G. Miao, B. Yuan, X. Chen, A facile synthesis of novel mesoporous bioactive glass nanoparticles with various morphologies and tunable mesostructure by sacrificial liquid template method, *Mater. Lett.* 148 (2015) 45–49.
- [39] M. Cámara-Torres, S. Duarte, R. Sinha, A. Egizabal, N. Álvarez, M. Bastianini, M. Sisani, P. Scopece, M. Scatto, A. Bonetto, A. Marcomini, A. Sanchez, A. Patelli, C. Mota, L. Moroni, 3D additive manufactured composite scaffolds with antibiotic-loaded lamellar fillers for bone infection prevention and tissue regeneration, *Bioact. Mater.* 6 (4) (2021) 1073–1082.
- [40] B. Byambaa, N. Annabi, K. Yue, G. Trujillo-de Santiago, M.M. Alvarez, W. Jia, M. Kazemzadeh-Narbat, S.R. Shin, A. Tamayol, A. Khademhosseini, Bioprinted osteogenic and vasculogenic patterns for engineering 3D bone tissue, *Adv Healthc Mater* 6 (16) (2017).
- [41] A.F. Chen, V.M. Schreiber, W. Washington, N. Rao, A.R. Evans, What is the rate of methicillin-resistant *Staphylococcus aureus* and Gram-negative infections in open fractures? *Clin. Orthop. Relat. Res.* 471 (10) (2013) 3135–3140.
- [42] H. Hourii, H. Kazemian, H. Sedigh Ebrahim-Saraie, A. Tajji, Z. Tayebi, H. Heidari, Linezolid activity against clinical Gram-positive cocci with advanced antimicrobial drug resistance in Iran, *J Glob Antimicrob Resist* 10 (2017) 200–203.
- [43] S. Tkachuk, K. Collins, M.H.H. Ensom, The relationship between vancomycin trough concentrations and AUC/MIC ratios in pediatric patients: a qualitative systematic review, *Paediatr Drugs* 20 (2) (2018) 153–164.
- [44] R. Diaz, V. Afreixo, E. Ramalheira, C. Rodrigues, B. Gago, Evaluation of vancomycin MIC creep in methicillin-resistant *Staphylococcus aureus* infections—a systematic review and meta-analysis, *Clin. Microbiol. Infect.* 24 (2) (2018).
- [45] M.J. Rybak, The pharmacokinetic and pharmacodynamic properties of vancomycin, *Clin. Infect. Dis.* 42 (Suppl 1) (2006) S35–S39.
- [46] Z. Neščáková, K. Zheng, L. Liverani, Q. Nawaz, D. Galusková, H. Kanková, M. Michálek, D. Galusek, A.R. Boccaccini, Multifunctional zinc ion doped sol-gel derived mesoporous bioactive glass nanoparticles for biomedical applications, *Bioact. Mater.* 4 (2019) 312–321.
- [47] K. Zheng, A.R. Boccaccini, Sol-gel processing of bioactive glass nanoparticles: a review, *Adv. Colloid Interface Sci.* 249 (2017) 363–373.
- [48] A.R. Boccaccini, M. Erol, W.J. Stark, D. Mohn, Z.K. Hong, J.F. Mano, Polymer/bioactive glass nanocomposites for biomedical applications: a review, *Compos. Sci. Technol.* 70 (13) (2010) 1764–1776.
- [49] Y. Cheng, Y. Gong, X. Chen, Q. Zhang, X. Zhang, Y. He, L. Pan, B. Ni, F. Yang, Y. Xu, L. Zhou, Y. Yang, W. Chen, Injectible adhesive hemostatic gel with tumor acidity neutralizer and neutrophil extracellular traps lyase for enhancing adoptive NK cell therapy prevents post-resection recurrence of hepatocellular carcinoma, *Biomaterials* 284 (2022), 121506.
- [50] L. Zhou, C. Dai, L. Fan, Y. Jiang, C. Liu, Z. Zhou, P. Guan, Y. Tian, J. Xing, X. Li, Y. Luo, P. Yu, C. Ning, G. Tan, Injectible self-healing natural biopolymer-based hydrogel adhesive with thermoresponsive reversible adhesion for minimally invasive surgery, *Adv. Funct. Mater.* 31 (14) (2021).
- [51] B. Sarker, W. Li, K. Zheng, R. Detsch, A.R. Boccaccini, Designing porous bone tissue engineering scaffolds with enhanced mechanical properties from composite hydrogels composed of modified alginate, gelatin, and bioactive glass, *ACS Biomater. Sci. Eng.* 2 (12) (2016) 2240–2254.
- [52] J. Qu, X. Zhao, Y. Liang, T. Zhang, P.X. Ma, B. Guo, Antibacterial adhesive injectable hydrogels with rapid self-healing, extensibility and compressibility as wound dressing for joints skin wound healing, *Biomaterials* 183 (2018) 185–199.
- [53] K.V. Tian, B. Yang, Y. Yue, D.T. Bowron, J. Mayers, R.S. Donnan, C. Dobó-Nagy, J. W. Nicholson, D.-C. Fang, A.L. Greer, G.A. Chass, G.N. Greaves, Atomic and vibrational origins of mechanical toughness in bioactive cement during setting, *Nat. Commun.* 6 (2015) 8631.
- [54] Y. Wang, L.-Q. Cai, B. Nugraha, Y. Gao, H.L. Leo, Current hydrogel solutions for repairing and regeneration of complex tissues, *Curr. Med. Chem.* 21 (22) (2014) 2480–2496.
- [55] G. Yan, S. He, G. Chen, S. Ma, A. Zeng, B. Chen, S. Yang, X. Tang, Y. Sun, F. Xu, L. Lin, X. Zeng, Highly flexible and broad-range mechanically tunable all-wood hydrogels with nanoscale channels via the Hofmeister effect for human motion monitoring, *Nano-Micro Lett.* 14 (1) (2022) 84.
- [56] T. Neubauer, G.S. Bayer, M. Wagner, Open fractures and infection, *Acta Chir. Orthop. Traumatol. Cech.* 73 (5) (2006) 301–312.
- [57] X. Zhao, P. Li, B. Guo, P.X. Ma, Antibacterial and conductive injectable hydrogels based on quaternized chitosan-graft-polyaniline/oxidized dextran for tissue engineering, *Acta Biomater.* 26 (2015) 236–248.
- [58] X. Zhao, H. Wu, B. Guo, R. Dong, Y. Qiu, P.X. Ma, Antibacterial anti-oxidant electroactive injectable hydrogel as self-healing wound dressing with hemostasis and adhesiveness for cutaneous wound healing, *Biomaterials* 122 (2017) 34–47.
- [59] J. Hoque, B. Bhattacharjee, R.G. Prakash, K. Paramanandham, J. Haldar, Dual function injectable hydrogel for controlled release of antibiotic and local antibacterial therapy, *Biomacromolecules* 19 (2) (2018) 267–278.
- [60] Y. Wang, Q. Zhao, N. Han, L. Bai, J. Li, J. Liu, E. Che, L. Hu, Q. Zhang, T. Jiang, S. Wang, Mesoporous silica nanoparticles in drug delivery and biomedical applications, *Nanomedicine* 11 (2) (2015) 313–327.
- [61] Z. Othman, B. Cillero Pastor, S. van Rijt, P. Habibovic, Understanding interactions between biomaterials and biological systems using proteomics, *Biomaterials* 167 (2018) 191–204.
- [62] C. Hou, Q. Yuan, D. Huo, S. Zheng, D. Zhan, Investigation on clotting and hemolysis characteristics of heparin-immobilized polyether sulfones biomembrane, *J. Biomed. Mater. Res.* 85 (3) (2008) 847–852.
- [63] Y. Tian, P. Guan, C. Wen, M. Lu, T. Li, L. Fan, Q. Yang, Y. Guan, X. Kang, Y. Jiang, C. Ning, R. Fu, G. Tan, L. Zhou, Strong biopolymer-based nanocomposite hydrogel adhesives with removability and reusability for damaged tissue closure and healing, *ACS Appl. Mater. Interfaces* 14 (49) (2022) 54488–54499.
- [64] K. Zheng, E. Torre, A. Bari, N. Taccardi, C. Cassinelli, M. Morra, S. Fiorilli, C. Vitale-Brovarone, G. Iviglia, A.R. Boccaccini, Antioxidant mesoporous Ce-doped bioactive glass nanoparticles with anti-inflammatory and pro-osteogenic activities, *Mater Today Bio* 5 (2020), 100041.
- [65] H. Takayanagi, Osteoimmunology: shared mechanisms and crosstalk between the immune and bone systems, *Nat. Rev. Immunol.* 7 (4) (2007) 292–304.
- [66] J.M. Sadowska, M.-P. Ginebra, Inflammation and biomaterials: role of the immune response in bone regeneration by inorganic scaffolds, *J. Mater. Chem. B* 8 (41) (2020) 9404–9427.
- [67] C. Vichery, J.-M. Nedelec, Bioactive glass nanoparticles: from synthesis to materials design for biomedical applications, *Materials* 9 (4) (2016).
- [68] Y. Liang, Z. Li, Y. Huang, R. Yu, B. Guo, Dual-dynamic-bond cross-linked antibacterial adhesive hydrogel sealants with on-demand removability for post-wound-closure and infected wound healing, *ACS Nano* 15 (4) (2021) 7078–7093.
- [69] N. Malachowa, S.D. Kobayashi, J. Lovaglio, F.R. DeLeo, Mouse model of *Staphylococcus aureus* skin infection, *Methods Mol. Biol.* 1960 (2019) 139–147.
- [70] N. Klopfenstein, J.E. Cassat, A. Monteith, A. Miller, S. Drury, E. Skaar, C. H. Serezani, Murine models for staphylococcal infection, *Curr Protoc* 1 (3) (2021) e52.
- [71] Y. Ma, Y. Sun, L. Xu, X. Li, D. Gong, Z. Miao, H. Qian, Pseudocatalytic hydrogels with intrinsic antibacterial and photothermal activities for local treatment of subcutaneous abscesses and breast tumors, *Adv Healthc Mater* (2022), e2201023.
- [72] S. Chen, Y. Tang, Y. Liu, P. Zhang, L. Lv, X. Zhang, L. Jia, Y. Zhou, Exosomes derived from miR-375-overexpressing human adipose mesenchymal stem cells promote bone regeneration, *Cell Prolif* 52 (5) (2019), e12669.